

Meson-Meson Scattering in the Quark Model: Spin Dependence and Exotic Channels

T.Barnes,^{1-4*} N.Black^{2†} and E.S.Swanson^{5,6‡}

¹*Physics Division, Oak Ridge National Laboratory*

Oak Ridge, TN 37831-6373, USA

²*Department of Physics and Astronomy, University of Tennessee*

Knoxville, TN 37996-1501, USA

³*Institut für Theoretische Kernphysik der Universität Bonn*

Nußallee 14-16, D-53115 Bonn, Germany

⁴*Forschungszentrum Jülich GmbH, Institut für Kernphysik*

D-52425 Jülich, Germany

⁵*Department of Physics and Astronomy, University of Pittsburgh,*

Pittsburgh, PA 15260, USA

⁶*Jefferson Laboratory, 12000 Jefferson Ave., Newport News, VA 23606, USA*

Abstract

We apply a quark interchange model to spin-dependent and exotic meson-meson scattering. The model includes the complete set of standard quark model forces, including OGE spin-orbit and tensor and scalar confinement spin-orbit. Scattering amplitudes derived assuming SHO and

*email: barnes@bethe.phy.ornl.gov

†email: nblack@nomad.phys.utk.edu

‡email: swansone@pitt.edu

Coulomb plus linear plus hyperfine meson wavefunctions are compared. In $I=2 \pi\pi$ we find approximate agreement with the S-wave phase shift from threshold to 1.5 GeV, where we predict an extremum that is supported by the data. Near threshold we find rapid energy dependence that may reconcile theoretical estimates of small scattering lengths with experimental indications of larger ones based on extrapolation of measurements at moderate k_π ². In PsV scattering we find that the quark-quark L·S and T forces map into L·S and T meson-meson interactions, and the P-wave L·S force is large. Finally we consider scattering in J^{PC_n} -exotic channels, and note that some of the “Deck effect” mechanisms suggested as possible nonresonant origins of the $\pi_1(1400)$ signal are not viable in this model.

I. INTRODUCTION

The determination of scattering amplitudes between pairs of mesons is an interesting problem in strong QCD. It is also a complicated problem, because both $q\bar{q}$ annihilation to s-channel resonances and “nonresonant” scattering are important effects, and it is often difficult to separate the various contributions. However by specializing to annihilation-free channels such as $I=2 \pi\pi$ and $\pi\rho$, $I=3/2 K\pi$, KN and NN, one may study nonresonant scattering in relative isolation. The determination of resonance parameters, reaction mechanisms, and many other aspects of hadron physics are complicated by the presence of nonresonant scattering, which is treated as an (often poorly understood) initial-state and final-state rescattering effect. Developing an accurate description of nonresonant scattering would help clarify many other aspects of hadron physics.

A further interesting possibility is that sufficiently attractive nonresonant scattering may lead to weakly bound hadron-hadron or multihadron states, as does happen in nuclei and hypernuclei. We may also find a rich spectrum of meson-meson bound states, the study of which will extend nuclear physics into the largely unexplored field of “mesonic

nuclei” or “molecules” [1–3].

An understanding of PsPs, PsV and other meson-meson scattering amplitudes is also important for the interpretation of non-QCD processes such as nonleptonic weak decays, since these show evidence of important hadronic final state interactions. The $\Delta I=1/2$ rule is a well known example. Similarly, a recent study of D and D_s decays to $K\bar{K}\pi$ [4] found that the Dalitz plots are dominated by two-meson isobars, including $\phi\pi$, $K^*\bar{K} + h.c.$ and $K_0^*(1430)\bar{K} + h.c.$, and complex relative amplitudes are required to describe the D^+ Dalitz plot. Without final state interactions one would expect relatively real couplings to these final states.

One finds a surprising variety of approaches to strong hadron-hadron scattering in the literature. There are many studies using effective hadronic lagrangians, such as the “chiral perturbation theory” description of the PsPs sector. Although this method is convenient because it uses perturbative QFT techniques, it is incomplete in that it takes effective lagrangian vertex strengths from the data; one should be able to calculate these hadronic couplings directly from quark-gluon forces.

Second, there are studies that model the low energy hadron-hadron scattering mechanism, which include the apparently dissimilar meson exchange and quark-gluon descriptions of hadronic forces. Meson exchange models are again attractive for their simplicity, since they use perturbative QFT techniques to determine scattering amplitudes. This approach has been elaborated in greatest detail in models of the NN force [5], in which a large number of meson exchanges is assumed. With this large parameter space a good description of this interaction is possible, although there is a concern that one may be parametrizing other scattering mechanisms in addition to t -channel meson exchange. Alternatively, one may calculate hadron-hadron forces directly from the fundamental quark-gluon interaction, using quark model hadron wavefunctions. This approach has also seen its most detailed development in studies of the NN interaction [6], and is most successful in describing the short-ranged repulsive core. Maltman and Isgur [6] also found a

physically reasonable intermediate ranged attraction from a color van der Waals effect in the quark-gluon approach, which is *not* equivalent to the usual $\pi\pi$ or σ meson exchange explanation of this force. The quark description of hadron-hadron interactions is complicated by the combinatorics of matrix elements between quark bound states, but has the advantage that it can easily be extended to a wide range of spin and flavor channels through a simple change of the external hadron wavefunctions.

A third promising approach is to infer hadron scattering amplitudes from LGT. To date LGT has seen little application to scattering problems because of the difficulty of treating systems that are not in their ground states. Estimates of the $I=0$ and $I=2$ $\pi\pi$ scattering lengths have been obtained by exploiting a theoretical relation to finite-size effects [7], and more recently very interesting results for nuclear physics potentials in the \mathcal{BB} system were reported [8]. In future it may be possible to improve hadron scattering models through comparisons with similar “LGT data”.

In this paper we are concerned with the derivation of meson-meson scattering amplitudes from quark-gluon forces. We derive meson-meson scattering amplitudes at lowest order in the quark-quark interaction, which leads to a quark interchange model described by “quark Born diagrams” [9,10]. Since the quark-quark interaction is already well established from hadron spectroscopy, our predictions have little parameter freedom. In previous work we and others (usually assuming OGE hyperfine dominance) have shown that this approach gives a reasonably accurate description of S-wave scattering in a wide range of channels without $q\bar{q}$ annihilation, including $I=2$ $\pi\pi$ [9], $I=3/2$ $K\pi$ [11], $I=0,1$ KN [12], $I=0,1$ BB [13] (compared to LGT data), and the NN repulsive core [6]. This approach has also been applied to $\pi J/\psi$ [14,15] and other reactions relevant to heavy ion collisions, where the experimental low energy cross sections are as yet unclear.

The principal new contribution of this paper is a detailed analytical derivation of the meson-meson scattering amplitudes that follow from the complete quark-quark interaction, including color Coulomb, linear scalar confinement, OGE spin-spin, OGE spin-orbit,

OGE tensor and linear spin-orbit forces. As a future application of these results, one might hope to clarify the relationship between meson exchange and quark interchange models by a detailed comparison of the spin dependence of hadron-hadron scattering amplitudes, which we expect to be sensitive to the details of the scattering mechanism.

Here we consider both pseudoscalar-pseudoscalar (PsPs) and pseudoscalar-vector (PsV) scattering. The former is a “standard benchmark” for meson scattering models, because I=2 $\pi\pi$ low energy scattering has no s -channel resonances and has been the subject of many experimental phase shift analyses. Although we find reasonable agreement with S-wave I=2 $\pi\pi$ scattering, this channel has no spin degree of freedom, and so cannot be used to test the characteristic spin dependences predicted by the quark model’s OGE and linear scalar confinement forces.

We find in contrast that PsV is an excellent theoretical laboratory for the study of spin-dependent forces, as it can accommodate both meson-meson spin-orbit and tensor interactions. The spin-dependent forces at the meson-meson level are closely related to the corresponding terms in the quark-quark interaction in our approach. Although the study of PsV scattering is essentially a theoretical exercise at present, these phase shifts are accessible experimentally, for example through measurement of the relative S and D final state phases in $b_1 \rightarrow \pi\omega$. Thus it should be possible to measure PsV phase shifts from resonance decays to multi-amplitude PsV final states.

Before we proceed to our detailed results, we note that some work has already appeared on meson-meson scattering in PsV systems. Numerical results for many light S-wave PsV meson channels were previously reported by Swanson [10] using a similar quark model approach that incorporated OGE spin-spin and linear confinement forces. Theoretical results for PsV scattering ($\pi\rho$ in particular) in a meson exchange model were published by Janssen *et al.* [16] and Böckmann *et al.* [17], assuming π , vector and a_1 exchange. Since the $\rho\pi\pi$, $a_1\rho\pi$ and $\rho\omega\pi$ vertex strengths are relatively well established, it was possible to evaluate these scattering amplitudes numerically. These papers did not consider the exotic

I=2 channel, so a direct comparison with our quark model PsV results is not possible at present.

II. MESON-MESON T-MATRIX

A. General T-matrix formula

We approximate the full hadron-hadron scattering amplitude by a single (Born-order) matrix element of the quark-quark interaction Hamiltonian H_I . Since H_I is $T^a T^a$ in color, one must then have quark line rearrangement to have a nonvanishing overlap with two color-singlet mesons in the final state. In $(q\bar{q}) - (q\bar{q})$ scattering there are four independent Born-order diagrams, which we label according to which pair of constituents interacted; these are “transfer₁” (T1), “transfer₂” (T2), “capture₁” (C1) and “capture₂” (C2), which are shown in Fig.1. In the special case of identical quarks *and* identical antiquarks, which is relevant here, there is a second set of four “symmetrizing” diagrams T1_{symm} . . . C2_{symm}, which are identical to T1 . . . C2 except that the quark lines are interchanged rather than the antiquark lines.

The hadron-hadron T-matrix element T_{fi} for each diagram can conveniently be written as an overlap integral of the meson wavefunctions times the underlying quark T_{fi} . These overlap integrals (specializing Ref. [13] to the case of equal quark and antiquark masses) are

$$\begin{aligned}
T_{fi}^{(\text{T1})}(AB \rightarrow CD) = & \\
& \iint d^3q d^3p \Phi_C^*(2\vec{p} + \vec{q} - \vec{C}) \Phi_D^*(2\vec{p} - \vec{q} - 2\vec{A} - \vec{C}) \\
& T_{fi}(\vec{q}, \vec{p}, \vec{p} - \vec{A} - \vec{C}) \Phi_A(2\vec{p} - \vec{q} - \vec{A}) \Phi_B(2\vec{p} + \vec{q} - \vec{A} - 2\vec{C}) , \quad (1)
\end{aligned}$$

$$\begin{aligned}
T_{fi}^{(\text{T2})}(AB \rightarrow CD) = & \\
& \iint d^3q d^3p \Phi_C^*(-2\vec{p} + \vec{q} + 2\vec{A} - \vec{C}) \Phi_D^*(-2\vec{p} - \vec{q} - \vec{C})
\end{aligned}$$

$$T_{fi}(\vec{q}, \vec{p}, \vec{p} - \vec{A} + \vec{C}) \Phi_A(-2\vec{p} + \vec{q} + \vec{A}) \Phi_B(-2\vec{p} - \vec{q} + \vec{A} - 2\vec{C}) . \quad (2)$$

$$\begin{aligned} T_{fi}^{(C1)}(AB \rightarrow CD) = \\ \iint d^3q d^3p \Phi_C^*(2\vec{p} + \vec{q} - \vec{C}) \Phi_D^*(2\vec{p} - \vec{q} - 2\vec{A} - \vec{C}) \\ T_{fi}(\vec{q}, \vec{p}, -\vec{p} + \vec{C}) \Phi_A(2\vec{p} - \vec{q} - \vec{A}) \Phi_B(2\vec{p} - \vec{q} - \vec{A} - 2\vec{C}) , \end{aligned} \quad (3)$$

$$\begin{aligned} T_{fi}^{(C2)}(AB \rightarrow CD) = \\ \iint d^3q d^3p \Phi_C^*(-2\vec{p} + \vec{q} + 2\vec{A} - \vec{C}) \Phi_D^*(-2\vec{p} - \vec{q} - \vec{C}) \\ T_{fi}(\vec{q}, \vec{p}, -\vec{p} - \vec{C}) \Phi_A(-2\vec{p} + \vec{q} + \vec{A}) \Phi_B(-2\vec{p} + \vec{q} + \vec{A} - 2\vec{C}) . \end{aligned} \quad (4)$$

The quark T_{fi} has momentum arguments $T_{fi}(\vec{q}, \vec{p}_1, \vec{p}_2)$, which are defined in Fig.2. In this paper we will evaluate these overlap integrals with standard Gaussian quark model wavefunctions and the quark T_{fi} for the complete set of OGE color Coulomb, linear scalar, OGE spin-spin, OGE and linear scalar confinement spin-orbit and OGE tensor interactions. These interactions are given in App.A.

B. PsPs Scattering

1. $I=2$ $\pi\pi$ T -matrix

We specialize the general problem of PsPs scattering without $q\bar{q}$ annihilation to $I=2$ $\pi\pi$ because many experiments have published phase shift analyses of this channel. The other $\pi\pi$ channels have large s -channel $q\bar{q}$ annihilation contributions. The full $I=2$ $\pi\pi$ Born-order T -matrix element is determined by adding the individual contributions of App.B, with PsPs spin matrix elements given in App.C, part C2. There are also flavor and color factors for each diagram and an overall “signature” phase of (-1) , and a second set of “symmetrizing” diagrams for identical quarks and identical antiquarks, as discussed in detail in Ref. [9]. On summing these contributions we find

$$\begin{aligned}
T_{fi}^{I=2 \pi\pi} = & + \frac{\pi\alpha_s}{m^2} \left(\frac{2^3}{3^2} \left(e^{-Q_+^2/8\beta^2} + e^{-Q_-^2/8\beta^2} \right) + \frac{2^7}{3^{7/2}} e^{-\vec{A}^2/3\beta^2} \right) \\
& + \frac{\pi\alpha_s}{\beta^2} \left(- \frac{2^4}{3^2} \left(f_{\frac{1}{2}, \frac{3}{2}}(\vec{Q}_+^2/8\beta^2) + f_{\frac{1}{2}, \frac{3}{2}}(\vec{Q}_-^2/8\beta^2) \right) + \frac{2^6}{3^{5/2}} f_{\frac{1}{2}, \frac{3}{2}}(\vec{A}^2/6\beta^2) \right) e^{-\vec{A}^2/2\beta^2} \\
& + \frac{\pi b}{\beta^4} \left(\frac{2^3}{3} \left(f_{-\frac{1}{2}, \frac{3}{2}}(\vec{Q}_+^2/8\beta^2) + f_{-\frac{1}{2}, \frac{3}{2}}(\vec{Q}_-^2/8\beta^2) \right) - \frac{2^3}{3^{1/2}} f_{-\frac{1}{2}, \frac{3}{2}}(\vec{A}^2/6\beta^2) \right) e^{-\vec{A}^2/2\beta^2} \quad (5)
\end{aligned}$$

where $f_{a,c}(x)$ is an abbreviation for the confluent hypergeometric (Kummer) function ${}_1F_1(a; c; x)$.

The three separate expressions above are the OGE spin-spin, color Coulomb and linear confinement contributions respectively. The Q_{\pm} terms come from the transfer diagrams, and the remaining, isotropic, terms come from the capture diagrams. The spin matrix elements of the spin-orbit and tensor terms vanish identically in the PsPs channel.

Since $\vec{Q}_{\pm} = \vec{C} \pm \vec{A}$ and $|\vec{A}| = |\vec{C}|$, one can equivalently write this amplitude as a function of the CM momentum and scattering angle using $\vec{Q}_{\pm}^2 = 2\vec{A}^2(1 \pm \mu)$, where $\mu = \cos(\theta_{AC})$. The Bose symmetry required for this $\pi\pi$ scattering amplitude is evident.

2. $I=2 \pi\pi$ Phase Shifts

We may derive the elastic Born-order $I=2 \pi\pi$ phase shifts from Eq.(5), using the relation between phase shifts and the T-matrix given in App.D, especially Eq.(D17), and the integrals in App.G. The result we find for the S-wave is

$$\delta_0^{I=2 \pi\pi} = \begin{cases} kE_{\pi} \frac{\alpha_s}{m^2} \left(-\frac{1}{3^2} \frac{1}{x} (1 - e^{-2x}) - \frac{2^4}{3^{7/2}} e^{-4x/3} \right) & \text{OGE spin-spin} \\ kE_{\pi} \frac{\alpha_s}{\beta^2} \left(-\frac{2}{3^2} \frac{1}{x} \left(f_{1, \frac{1}{2}}(-2x) - e^{-2x} \right) - \frac{2^3}{3^{5/2}} f_{1, \frac{3}{2}}(-2x/3) e^{-4x/3} \right) & \text{OGE color Cou.} \\ kE_{\pi} \frac{b}{\beta^4} \left(\frac{1}{3^2} \frac{1}{x} \left(f_{2, \frac{1}{2}}(-2x) - e^{-2x} \right) + \frac{1}{3^{1/2}} f_{2, \frac{3}{2}}(-2x/3) e^{-4x/3} \right) & \text{linear conf.} \end{cases} \quad (6)$$

where we have introduced $x = \vec{A}^2/4\beta^2$. The total Born-order S-wave phase shift is the sum of these three contributions.

This S-wave phase shift is shown in Fig.3 with our standard quark model parameter set $\alpha_s = 0.6$, $\beta = 0.4$ GeV, $m = 0.33$ GeV and $b = 0.18$ GeV². We also use $M_{\pi} = 0.138$ GeV

throughout. This confirms that the color Coulomb and linear confinement interactions make relatively small contributions to the I=2 $\pi\pi$ S-wave at moderate energies. The weakly repulsive linear confining interaction in I=2 $\pi\pi$ near threshold was previously found numerically by Swanson [10].

One might be concerned about the approximation of using SHO wavefunctions, especially at higher energy scales where there should be strong short-distance components in the pion wavefunction due to the attractive spin-spin hyperfine interaction. To test the sensitivity to SHO wavefunctions we evaluated the I=2 $\pi\pi$ scattering amplitudes and phase shifts numerically using Coulomb plus linear plus hyperfine $q\bar{q}$ wavefunctions and Monte Carlo integration of the real space integrals corresponding to the T-matrix integrals (1-4). As usual this requires a “smearing” of the contact hyperfine term, $\delta(\vec{x}) \rightarrow e^{-\sigma^2 r^2} / \pi^{3/4} \sigma^{3/2}$, to allow solution of the Schrödinger equation with an attractive delta-function interaction. In the literature the inverse smearing length is typically taken to be $\sigma \approx 1$ GeV. (A calculation of I=2 $\pi\pi$ scattering with this interaction and $\sigma = 0.7$ GeV was reported previously by Swanson [10].) With our standard light-quark parameter set $\alpha_s = 0.6$, $b = 0.18$ GeV² and $m = 0.33$ GeV, we found that fitting the $M_\rho - M_\pi$ splitting required a value of $\sigma = 0.86$ GeV. To illustrate the dependence of the scattering amplitude on this parameter, in Fig.4 we show the I=2 $\pi\pi$ S-wave that follows from our standard quark model set (α_s, b, m) , with $\sigma = 0.7, 0.8$ and 0.9 GeV. Clearly the predicted phase shift is rather similar to the SHO result of Fig.3, although the effect of short-distance peaking in the π wavefunction is evident above $M_{\pi\pi} \approx 1$ GeV.

We also show most of the higher statistics experimental results for the I=2 $\pi\pi$ S-wave phase shift in Figs.3 and 4. The references shown are Colton *et al.* [18], Durusoy *et al.* [19] (OPE extrapolation, solid; OPE + DP form factor, open, slightly displaced in x for visibility), Hoogland *et al.* [20] (extrapolation B), and Losty *et al.* [21]. Prukop *et al.* [22] found a wide range of results from three different off-shell extrapolations, so we simply quote their fitted scattering length below.

Clearly there is already reasonable agreement with the experimental S-wave phase shift at lower energies without fitting the quark model parameters. The model predicts a rather dramatic extremum in this phase shift near $M_{\pi\pi} = 1.5$ GeV, which is unfortunately beyond the limiting invariant mass of most of the experimental studies. There are some measurements of this phase shift at higher invariant mass with lower accuracy due to Durusoy *et al.* [19], which are also shown in the figure. The Durusoy *et al.* results support our predicted extremum near $M_{\pi\pi} = 1.5$ GeV; indeed, their phase shift above $M_{\pi\pi} = 1.5$ GeV appears to fall even more rapidly than we predict.

We have investigated optimal parameter fits of the S-wave phase shift formula Eq.(6) to the data, but we find that these are rather unstable because the color Coulomb and linear confinement contributions are small and are qualitatively similar functions. In any case the Durusoy *et al.* data and Fig.4 show that the hyperfine smearing distance σ is an important parameter, and this will not be well determined until accurate phase shift data becomes available at higher invariant mass. An accurate measurement of I=2 $\pi\pi$ scattering amplitudes near and above $M_{\pi\pi} = 1.5$ GeV would clearly be very useful as a test of this and other models of meson-meson scattering.

3. I=2 $\pi\pi$ Scattering Lengths

The I=2 $\pi\pi$ scattering length is defined by $a_0^{I=2} = \lim_{k_\pi \rightarrow 0} \delta_0^{I=2 \pi\pi} / k_\pi$. The results we find from Eq.(6) are

$$a_0^{I=2} = \begin{cases} -\frac{2}{3^2} \left(1 + \frac{2^3}{3^{3/2}}\right) \frac{\alpha_s}{m^2} M_\pi & S \cdot S \\ -\frac{2^2}{3^2} \left(\frac{2}{3^{1/2}} - 1\right) \frac{\alpha_s}{\beta^2} M_\pi & \text{Cou.} \\ -\frac{2}{3} \left(1 - \frac{3^{1/2}}{2}\right) \frac{b}{\beta^4} M_\pi & \text{lin.} \end{cases} \quad (7)$$

and their numerical values with our standard quark model parameters set are

$$a_0^{I=2} = \begin{cases} -0.085 \text{ [fm]} & S \cdot S \\ -0.007 \text{ [fm]} & \text{Cou.} \\ -0.017 \text{ [fm]} & \text{lin.} \\ -0.109 \text{ [fm]} & \text{total.} \end{cases} \quad (8)$$

The Coulomb and linear contributions were independently checked by Monte Carlo integration of the corresponding real-space overlap integrals. The relative sizes of these numerical contributions *a posteriori* justify the approximation of neglecting the color Coulomb and linear terms in I=2 $\pi\pi$ scattering.

The I=2 $\pi\pi$ scattering length has been calculated previously using many other theoretical approaches. A summary of some of these predictions is given below. (We use a current value of $f_\pi = 93$ MeV in Weinberg's PCAC formula $a_0^{I=2} = -M_\pi/16\pi f_\pi^2$.)

$$a_0^{I=2} \Big|_{thy.} = \begin{cases} -0.053(7) \text{ [fm]} & \text{LGT [7]} \\ -0.052 \text{ [fm]} & \text{meson exchange [23,24]} \\ -0.053 \text{ [fm]} & \text{Roy Eqs. [25]} \\ -0.063 \text{ [fm]} & \text{PCAC [26].} \end{cases} \quad (9)$$

Although f_π and other effective lagrangian parameters are normally taken from experiment, these parameters are of course calculable from quark-gluon forces. As an example, our result for $a_0^{I=2}$ yields the following expression for f_π ,

$$\frac{1}{f_\pi^2} = \frac{2^5}{3^2} \left(1 + \frac{2^3}{3^{3/2}}\right) \frac{\pi\alpha_s}{m^2} + \frac{2^6}{3^2} \left(\frac{2}{3^{1/2}} - 1\right) \frac{\pi\alpha_s}{\beta^2} + \frac{2^5}{3} \left(1 - \frac{3^{1/2}}{2}\right) \frac{\pi b}{\beta^4}. \quad (10)$$

The dominant contribution comes from the $O(\alpha_s/m^2)$ OGE $S \cdot S$ term.

Experimental determinations of the scattering length have yielded results which are larger than theoretical expectations;

$$a_0^{I=2} \Big|_{expt.} = \begin{cases} -0.13(2) \text{ [fm]} & \text{Losty } et al. [21] \\ -0.24(2), -0.22_{-0.04}^{+0.03} \text{ [fm]} & \text{Prukop } et al. [22] . \end{cases} \quad (11)$$

We speculate that this discrepancy is due to the use of a simple $\delta = k_\pi a + O(k_\pi^3)$ effective range formula in extrapolation. The difficulty of extrapolating experimental phase shifts to threshold has been stressed by Morgan and Pennington [27,28]. We advocate the use

of a “generalized specific heat plot” of low energy phase shifts for this purpose [12]. This plot takes into account the threshold behavior seen in Eq.(6),

$$\delta_0^{I=2\pi\pi} = k_\pi E_\pi f(\alpha_s, m, b, \beta, x) \quad (12)$$

where f is a relatively slowly varying function of $x = k_\pi^2/4\beta^2$. Thus the threshold behavior is approximately proportional to $k_\pi E_\pi$ rather than just k_π , and since M_π is quite small this leads to rapid variation near threshold and makes the linear- k_π extrapolation inaccurate. We suggest removal of all this dependence by displaying $\delta_0/(k_\pi E_\pi/M_\pi)$ versus k_π^2 . The intercept in this plot is the scattering length, and the slope at intercept implies the effective range.

This generalized specific heat plot is shown in Fig.5 for $I=2$ $\pi\pi$ scattering. An extrapolation of the moderate- k_π data can now be seen to be much closer to the theoretical scattering lengths. The small- k_π dependence of δ_0/k_π was calculated by Donoghue [29] in a chiral effective lagrangian, which gave the Weinberg result at $k_\pi = 0$ and an $O(k_\pi^2)$ correction factor of $(1 + k_\pi^2/2m_\pi^2)$. This is just the correction due to an overall factor of E_π , so this predicts a zero slope in k_π^2 for $\delta_0/(k_\pi E_\pi/M_\pi)$ at threshold.

The Jülich meson-exchange model [23], which is dominated by t -channel ρ exchange in this process, also predicts rapid variation in δ_0/k_π near threshold. The prediction of this model for $\delta_0/(k_\pi E_\pi/M_\pi)$ [24], shown in Fig.5, is rather similar to our quark model result.

4. $I=2$ $\pi\pi$ Equivalent Potentials

Low energy “phase shift equivalent” Gaussian $I=2$ $\pi\pi$ potentials, derived using the method of Mott and Massey [30] as described in App.E, are given below. We quote separate Gaussians for the transfer and capture contributions from each of the three interactions, spin-spin contact, color Coulomb and linear hyperfine. However their predicted phase shift decays more slowly at large momentum, probably due to the use of power law

form factors in their vertices.

$$V_{\pi\pi}(r) = \begin{cases} +\frac{2^{9/2}}{3^2\pi^{1/2}} \frac{\alpha_s\beta^3}{m^2} e^{-2\beta^2 r^2} & S \cdot S \text{ (transfer)} \\ +\frac{2^{9/2}}{3^2\pi^{1/2}} \frac{\alpha_s\beta^3}{m^2} e^{-\frac{3}{2}\beta^2 r^2} & S \cdot S \text{ (capture)} \\ -\frac{2^{11/2}}{3^{1/2}5^{3/2}\pi^{1/2}} \alpha_s\beta e^{-\frac{6}{5}\beta^2 r^2} & \text{Cou. (transfer)} \\ +\frac{2^{1/2}3^{1/2}}{\pi^{1/2}} \alpha_s\beta e^{-\frac{9}{8}\beta^2 r^2} & \text{Cou. (capture)} \\ +\frac{2^{9/2}3^{1/2}}{7^{3/2}\pi^{1/2}} \frac{b}{\beta} e^{-\frac{6}{7}\beta^2 r^2} & \text{lin. (transfer)} \\ -\frac{2^{1/2}3^{5/2}}{5^{3/2}\pi^{1/2}} \frac{b}{\beta} e^{-\frac{9}{10}\beta^2 r^2} & \text{lin. (capture)}. \end{cases} \quad (13)$$

In Ref. [9] we derived $I=2$ $\pi\pi$ potentials for the spin-spin contact interaction using the ‘‘locality expansion’’ method of Ref. [31]. This gave an identical result for the spin-spin transfer potential, because this amplitude (before Bose symmetrization) is a function of t only. However for the capture diagrams the Mott-Massey approach used here gives a different potential, since it is constrained to reproduce the $O(k^3)$ series expansion of the phase shift in Eq.(6), but the local approximation is not. The two capture potentials reproduce the scattering length, but the local approximation gives an incorrect effective range.

The low energy Mott-Massey $I=2$ $\pi\pi$ potential is shown in Fig.6 for our standard quark model parameters $\alpha_s = 0.6$, $b = 0.18 \text{ GeV}^2$ and $m = 0.33 \text{ GeV}$. The spin-spin hyperfine contribution is dominant over the range shown.

5. $I=2$ $\pi\pi$ Phase Shifts with $L > 0$

The higher partial waves ($L \geq 2$) may be evaluated similarly. According to Eq.(5), these receive contributions only from the transfer diagrams. The Born-order D-wave phase shift with SHO wavefunctions is given by

$$\delta_2^{I=2} \pi\pi = \begin{cases} kE_\pi \frac{\alpha_s}{m^2} \left(-\frac{1}{3^2} \frac{1-e^{-2x}}{x} + \frac{1}{3} \frac{1+e^{-2x}}{x^2} - \frac{1}{3} \frac{1-e^{-2x}}{x^3} \right) & S \cdot S \\ kE_\pi \frac{\alpha_s}{\beta^2} \left(-\frac{2}{3^2} \frac{f_{1,\frac{1}{2}}(-2x)-e^{-2x}}{x} + \frac{2}{3^2} \frac{f_{1,-\frac{1}{2}}(-2x)+e^{-2x}}{x^2} - \frac{2}{3 \cdot 5} \frac{f_{1,-\frac{3}{2}}(-2x)-e^{-2x}}{x^3} \right) & \text{Cou.} \\ kE_\pi \frac{b}{\beta^4} \left(\frac{1}{3} \frac{f_{2,\frac{1}{2}}(-2x)-e^{-2x}}{x} - \frac{1}{5} \frac{f_{2,-\frac{1}{2}}(-2x)+e^{-2x}}{x^2} + \frac{3}{5 \cdot 7} \frac{f_{2,-\frac{3}{2}}(-2x)-e^{-2x}}{x^3} \right) & \text{lin.} \end{cases} \quad (14)$$

These three expressions are numerically rather small, and their phases are such that they approximately cancel; at $M_{\pi\pi} = 1.5$ GeV they are respectively -0.8° , $+0.2^\circ$ and $+0.4^\circ$. To see this more clearly, the leading $O(k_\pi^5)$ behavior predicted by Eq.(14) is

$$\lim_{k_\pi \rightarrow 0} \delta_2^{I=2 \pi\pi} / k_\pi^5 = \frac{1}{2^3 3^3 5^2} \left(-5 \frac{\alpha_s \beta^2}{m^2} + 2 \alpha_s + 3 \frac{b}{\beta^2} \right) \frac{M_\pi}{\beta^6}, \quad (15)$$

and the three dimensionless combinations $\alpha_s \beta^2 / m^2$, α_s and b / β^2 are comparable in size. We have also evaluated this D-wave phase shift using Coulomb plus linear plus hyperfine wavefunctions. The result is shown in Fig.4, and is numerically similar to the SHO D-wave, Eq.(14).

In comparison the experimental D-waves reported by Durusoy *et al.* [19] and Hoogland *et al.* [20] are $\approx -3^\circ$ at $M_{\pi\pi} = 1.5$ GeV (see Fig.4). (Losty *et al* [21] report a rather larger but inconsistent low-energy D-wave.) This is clearly larger than our prediction, although the rather slow variation of the Durusoy *et al.* and Hoogland *et al.* D-waves with $M_{\pi\pi}$ may indicate a problem with the measurements; the expected threshold behavior of k_π^5 is much more rapid than the observed energy dependence. Unfortunately the dispersion relations represented by the Roy equations have technical difficulties with determining D- and higher waves [25]. They do however lead to predictions of a *positive* D-wave close to threshold, which is not evident in the data. The D-wave may well have important meson exchange contributions, since this type of model can accommodate the reported experimental phase shift [32].

C. PsV Scattering

1. $I=2 \pi\rho$ T -matrix

For simplicity we will initially quote results only for $I=2 \pi\rho$. The other isospin channels are simply related by flavor factors, which we will discuss subsequently. We assume identical spatial wavefunctions, so only the ρ spin degree of freedom and difference in phase space distinguish this case from $\pi\pi$. Summing the individual contributions in

App.B with the appropriate flavor and color factors and the (-1) signature phase, and using the PsV spin matrix elements of App.C part C3, we find for the $I=2$ $\pi\rho$ T-matrix

$$\begin{aligned}
T_{fi}^{I=2 \pi\rho} = & \\
& + \frac{\pi\alpha_s}{m^2} \left(+ \frac{2^3}{3^3} \left(3 e^{-\vec{Q}_-^2/8\beta^2} - e^{-\vec{Q}_+^2/8\beta^2} \right) + \frac{2^7}{3^{9/2}} e^{-\vec{A}^2/3\beta^2} \right) \\
& + \frac{\pi\alpha_s}{\beta^2} \left(- \frac{2^4}{3^2} \left(f_{\frac{1}{2}, \frac{3}{2}}(\vec{Q}_-^2/8\beta^2) + f_{\frac{1}{2}, \frac{3}{2}}(\vec{Q}_+^2/8\beta^2) \right) + \frac{2^6}{3^{5/2}} f_{\frac{1}{2}, \frac{3}{2}}(\vec{A}^2/6\beta^2) \right) e^{-\vec{A}^2/2\beta^2} \\
& + \frac{\pi b}{\beta^4} \left(+ \frac{2^3}{3} \left(f_{-\frac{1}{2}, \frac{3}{2}}(\vec{Q}_-^2/8\beta^2) + f_{-\frac{1}{2}, \frac{3}{2}}(\vec{Q}_+^2/8\beta^2) \right) - \frac{2^3}{3^{1/2}} f_{-\frac{1}{2}, \frac{3}{2}}(\vec{A}^2/6\beta^2) \right) e^{-\vec{A}^2/2\beta^2} \\
& + \frac{\pi\alpha_s}{m^2\beta^2} \left(- \frac{2^2}{3^2} f_{\frac{3}{2}, \frac{5}{2}}(\vec{Q}_+^2/8\beta^2) - \frac{2^4}{3^{9/2}} f_{\frac{3}{2}, \frac{5}{2}}(\vec{A}^2/6\beta^2) \right) e^{-\vec{A}^2/2\beta^2} \left[\vec{S}_\rho \cdot i(\vec{A} \times \vec{C}) \right] \\
& + \frac{\pi b}{m^2\beta^4} \left(+ \frac{2}{3^2} f_{\frac{1}{2}, \frac{5}{2}}(\vec{Q}_+^2/8\beta^2) - \frac{2}{3^{5/2}} f_{\frac{1}{2}, \frac{5}{2}}(\vec{A}^2/6\beta^2) \right) e^{-\vec{A}^2/2\beta^2} \left[\vec{S}_\rho \cdot i(\vec{A} \times \vec{C}) \right] \\
& + \frac{\pi\alpha_s}{m^2\beta^2} \left(+ \frac{2}{3^2 \cdot 5} f_{\frac{5}{2}, \frac{7}{2}}(\vec{Q}_-^2/8\beta^2) \right) e^{-\vec{A}^2/2\beta^2} \left[\vec{S}_\rho \cdot \vec{Q}_- \vec{S}_\rho \cdot \vec{Q}_- - \frac{2}{3} \vec{Q}_-^2 \right] \\
& + \frac{\pi\alpha_s}{m^2\beta^2} \left(+ \frac{2^5}{3^{9/2} \cdot 5} f_{\frac{5}{2}, \frac{7}{2}}(\vec{A}^2/6\beta^2) \right) e^{-\vec{A}^2/2\beta^2} \left[\left[\vec{S}_\rho \cdot \vec{A} \vec{S}_\rho \cdot \vec{A} - \frac{2}{3} \vec{A}^2 \right] + \left[\vec{S}_\rho \cdot \vec{C} \vec{S}_\rho \cdot \vec{C} - \frac{2}{3} \vec{C}^2 \right] \right].
\end{aligned} \tag{16}$$

The individual contributions in this result are respectively OGE spin-spin; OGE color Coulomb; linear confinement; OGE spin-orbit; linear scalar confinement spin-orbit; OGE tensor (transfer diagrams); and OGE tensor (capture diagrams). In all these we list transfer followed by capture contributions. \vec{S}_ρ is the ρ meson spin vector, \vec{A} and \vec{C} are the initial and final π momenta, $\vec{B} = -\vec{A}$ and $\vec{D} = -\vec{C}$ are the initial and final ρ momenta, and $\vec{Q}_\pm = \vec{C} \pm \vec{A}$ as in $\pi\pi$. Since this result was derived in the CM frame, $|\vec{A}| = |\vec{B}| = |\vec{C}| = |\vec{D}|$. This T_{fi} evidently describes $\pi\rho$ spin-orbit and tensor interactions,

in addition to spin-independent scattering. It is interesting that there is a one-to-one mapping between the quark-quark spin-orbit and tensor interactions and these $\pi\rho$ spin-orbit and tensor terms. This simple result need not be true in general; a given spin-dependent interaction at the quark level may give rise to a different type of hadron-hadron interaction. As an example, a mapping of a tensor nucleon-nucleon force into a nucleon-nucleus spin-orbit interaction was discussed by Stancu, Brink and Flocard. [33]

To evaluate phase shifts and inelasticities it is convenient to calculate the matrix element of our $\pi\rho$ T-matrix Eq.(16) between general $|jls\rangle$ states, which gives the reduced matrix element

$$T_{l'l}^j \equiv \langle jm, l's | T | jm, ls \rangle =$$

$$\sum_{\substack{\mu\mu' \\ s_z s'_z}} \langle jm | l'\mu', 1s'_z \rangle \langle jm | l\mu, 1s_z \rangle \iint d\Omega' d\Omega Y_{l'\mu'}^*(\Omega') \langle 1s'_z | T_{fi}(\Omega', \Omega) | 1s_z \rangle Y_{l\mu}(\Omega), \quad (17)$$

as discussed in App.D. This is a straightforward exercise, although integrals of special functions and a careful angular analysis of the spin-orbit and tensor terms are required; the details are discussed in Apps.G and H. This matrix element is diagonal in l except for the tensor interaction, which has both diagonal and off-diagonal (transfer) and fully off-diagonal (capture) contributions. The l -diagonal results, again showing transfer diagram contributions followed by capture, are

$$T_{ll}^j|_{S.S} = \frac{\pi^2 \alpha_s}{m^2} \left((1 + \delta_{l,odd}) \frac{2^6}{3^3} i_l(x) e^{-x} + \delta_{l,0} \frac{2^9}{3^{9/2}} e^{-4x/3} \right) \quad (18)$$

$$T_{ll}^j|_{Cou.} = \frac{\pi^2 \alpha_s}{\beta^2} \left(-\delta_{l,even} \frac{2^6}{3^2} \mathcal{F}_{\frac{1}{2}, \frac{3}{2}}^{(l)}(x) + \delta_{l,0} \frac{2^8}{3^{5/2}} f_{\frac{1}{2}, \frac{3}{2}}(2x/3) \right) e^{-2x} \quad (19)$$

$$T_{ll}^j|_{lin.} = \frac{\pi^2 b}{\beta^4} \left(\delta_{l,even} \frac{2^5}{3} \mathcal{F}_{-\frac{1}{2}, \frac{3}{2}}^{(l)}(x) - \delta_{l,0} \frac{2^5}{3^{1/2}} f_{-\frac{1}{2}, \frac{3}{2}}(2x/3) \right) e^{-2x} \quad (20)$$

$$T_{ll}^j|_{OGE\ L-S} = \frac{\pi^2 \alpha_s}{m^2} \langle \vec{L} \cdot \vec{S} \rangle \cdot \left(-\frac{2^5}{3^2} \frac{1}{(2l+1)} x \left(\mathcal{F}_{\frac{3}{2}, \frac{5}{2}}^{(l-1)}(x) - \mathcal{F}_{\frac{3}{2}, \frac{5}{2}}^{(l+1)}(x) \right) - \delta_{l,1} \frac{2^8}{3^{11/2}} x f_{\frac{3}{2}, \frac{5}{2}}(2x/3) \right) e^{-2x} \quad (21)$$

$$T_{ll}^j|_{lin.\ L-S} = \frac{\pi^2 b}{m^2 \beta^2} \langle \vec{L} \cdot \vec{S} \rangle \cdot \left(\frac{2^4}{3^2} \frac{1}{(2l+1)} x \left(\mathcal{F}_{\frac{1}{2}, \frac{5}{2}}^{(l-1)}(x) - \mathcal{F}_{\frac{1}{2}, \frac{5}{2}}^{(l+1)}(x) \right) - \delta_{l,1} \frac{2^5}{3^{7/2}} x f_{\frac{1}{2}, \frac{5}{2}}(2x/3) \right) e^{-2x} \quad (22)$$

$$T_{ll}^j|_{OGE\ T}^{transfer} = \frac{\pi^2 \alpha_s}{m^2} \langle T \rangle \cdot (-1)^{l+1} \frac{2^4}{3^3 \cdot 5} x \left(\frac{l}{(2l+1)} \mathcal{F}_{\frac{5}{2}, \frac{7}{2}}^{(l-1)}(x) + \frac{2l}{(2l+3)} \mathcal{F}_{\frac{5}{2}, \frac{7}{2}}^{(l)}(x) + \frac{l(2l-1)}{(2l+1)(2l+3)} \mathcal{F}_{\frac{5}{2}, \frac{7}{2}}^{(l+1)}(x) \right) e^{-2x} \quad (23)$$

and the off-diagonal tensor matrix elements are

$$T_{l' \neq l}^j|_{OGE\ T}^{transfer} = \frac{\pi^2 \alpha_s}{m^2} \left(\delta_{l, j-1} \delta_{l', j+1} + \delta_{l, j+1} \delta_{l', j-1} \right) \cdot (-1)^{j+1} \frac{2^4}{3^2 \cdot 5} \frac{[j(j+1)]^{1/2}}{(2j+1)} x \left(\mathcal{F}_{\frac{5}{2}, \frac{7}{2}}^{(j-1)}(x) + 2\mathcal{F}_{\frac{5}{2}, \frac{7}{2}}^{(j)}(x) + \mathcal{F}_{\frac{5}{2}, \frac{7}{2}}^{(j+1)}(x) \right) e^{-2x} \quad (24)$$

$$T_{l' \neq l}^j|_{OGE\ T}^{capture} = \frac{\pi^2 \alpha_s}{m^2} \delta_{j1} \left(\delta_{l2} \delta_{l'0} + \delta_{l0} \delta_{l'2} \right) \frac{2^{19/2}}{3^{11/2} \cdot 5} x f_{\frac{5}{2}, \frac{7}{2}}(2x/3) e^{-2x} . \quad (25)$$

In these formulas $i_l(x)$ is a modified spherical Bessel function, the tensor $\langle T \rangle$ matrix element between $|j, l, s=1\rangle$ $\pi\rho$ states is

$$\langle T \rangle = \begin{cases} 1 & j = l + 1 \\ -(2l+3)/l & j = l \\ (l+1)(2l+3)/l(2l-1) & j = l - 1 \end{cases} , \quad (26)$$

and the integral

$$\mathcal{F}_{a,c}^{(l)}(x) \equiv \int_{-1}^1 d\mu P_l(\mu) {}_1F_1(a; c; x(1+\mu)) \quad (27)$$

is evaluated in App.G.

2. $I=2$ $\pi\rho$ S-wave Phase Shifts

In S-wave to S-wave scattering the spin-orbit and tensor $\pi\rho$ T-matrix contributions vanish, and we are left with color Coulomb, linear and spin-spin contributions, just as in the $I=2$ $\pi\pi$ case. The $I=2$ $\pi\rho$ S-wave phase shifts that result from these interactions, again using Eq.(D17), are

$$\delta_0^{I=2 \pi\rho} = \begin{cases} \frac{kE_\pi E_\rho}{\sqrt{s}} \frac{\alpha_s}{m^2} \left(-\frac{2^2}{3^3} \frac{1}{x} (1 - e^{-2x}) - \frac{2^6}{3^{9/2}} e^{-4x/3} \right) & S \cdot S \\ \frac{kE_\pi E_\rho}{\sqrt{s}} \frac{\alpha_s}{\beta^2} \left(-\frac{2^3}{3^2} \frac{1}{x} (f_{1, \frac{1}{2}}(-2x) - e^{-2x}) - \frac{2^5}{3^{5/2}} f_{1, \frac{3}{2}}(-2x/3) e^{-4x/3} \right) & \text{Cou.} \\ \frac{kE_\pi E_\rho}{\sqrt{s}} \frac{b}{\beta^4} \left(\frac{2^2}{3^2} \frac{1}{x} (f_{2, \frac{1}{2}}(-2x) - e^{-2x}) + \frac{2^2}{3^{1/2}} f_{2, \frac{3}{2}}(-2x/3) e^{-4x/3} \right) & \text{lin.} \end{cases} \quad (28)$$

where $\sqrt{s} = (E_\pi + E_\rho)$, and again $x = \vec{A}^2/4\beta^2$. In Fig.6 we show these individual components and the total S-wave phase shift with our standard quark model parameter set and meson masses (used throughout) of $M_\pi = 0.138$ GeV and $M_\rho = 0.77$ GeV. The forces considered here evidently lead to strong repulsion in the $I=2$ $\pi\rho$ channel.

3. $I=2$ $\pi\rho$ Phase Shifts with $L > 0$

The spin-orbit and tensor terms in Eqs.(21-23) all contribute to $l > 0$ $\pi\rho$ scattering, and there is also an odd- l , j -independent term due to the OGE spin-spin interaction in Eq.(18), which is not symmetric under $\mu \rightarrow -\mu$. The color Coulomb and linear confinement spin-independent terms, Eqs.(19,20), contribute only to even l .

Adding the various diagonal matrix elements of Eqs.(18-23) and using Eq.(D17) gives phase shifts for each 3L_J partial wave. In Fig.8 we show results for all P-wave channels and for $J=L\pm 1$ in D- and F-wave. Note that there is a large, inverted spin-orbit force in the P-wave, so the 3P_0 phase shift is widely separated from 3P_2 , and has an even larger maximum phase shift than the S-wave. The higher-L channels show decreasing phase shifts with increasing L, as expected for short-ranged quark-gluon forces.

The relative importance of the individual contributions to the spin-dependent force is of considerable interest. In Fig.9 we show the various spin-dependent contributions

to the $I=2$ 3P_2 $\pi\rho$ phase shift. The largest contribution arises from OGE spin-orbit, in particular from the transfer diagrams. The OGE and confinement spin-orbit capture diagrams give smaller contributions of the same sign. Finally, the confinement spin-orbit transfer diagrams have a sign opposite to all these and reduces the total spin-orbit force somewhat. This dominance of the PsV spin-orbit by OGE is an interesting result, especially since Mukhopadhyay and Pirner [34] found the opposite result in KN. In that system they concluded that confinement, not OGE, makes the largest contribution to the spin-orbit force. The OGE tensor in $I=2$ 3P_2 $\pi\rho$ is weakly repulsive; it makes a much larger contribution to 3P_1 and 3P_0 , where the tensor matrix element is respectively -5 and 10 times as large. The OGE tensor is evident in Fig.8, in the departure of the ratio $({}^3P_2 - {}^3P_1):({}^3P_1 - {}^3P_0)$ from the pure spin-orbit value of $2:1$ at higher energies.

There is also an off-diagonal coupling due to the OGE tensor terms, given by Eqs.(24,25), but we have neglected this in calculating phase shifts because we find that it is numerically a small effect. The largest coupling at low energies is ${}^3S_1 \leftrightarrow {}^3D_1$, which leads to an inelasticity of only $\eta_{SD} = 0.97$ by $M_{\pi\rho} = 3.0$ GeV (calculated using Eqs.(D18-D20)).

4. $I=2$ $\pi\rho$ P-wave Spin-Orbit Potentials

We may determine low energy Gaussian equivalent $\pi\rho$ potentials from the phase shifts, as discussed in App.E. The most interesting potential phenomenologically is the spin-orbit one, since the origin of the spin-orbit interaction in the NN system is a long-standing and still poorly understood problem. In particular we derived Gaussian potentials corresponding to the P-wave phase shifts due to the OGE and linear scalar confinement spin-orbit interactions, using Eq.(E4) of App.E. The results for the transfer and capture contributions to these potentials are

$$V_{\pi\rho}^{s.o.}(r) = \begin{cases} -\frac{2^{11/2}5^{5/2}}{3^2 7^{5/2} \pi^{1/2}} \frac{\alpha_s \beta^3}{m^2} \langle \vec{L} \cdot \vec{S} \rangle e^{-\frac{10}{7}\beta^2 r^2} & \text{OGE (transfer)} \\ -\frac{5^{5/2}}{3^{9/2} \pi^{1/2}} \frac{\alpha_s \beta^3}{m^2} \langle \vec{L} \cdot \vec{S} \rangle e^{-\frac{5}{4}\beta^2 r^2} & \text{OGE (capture)} \\ +\frac{2^{9/2}5^{5/2}}{3^7 \pi^{1/2}} \frac{b\beta}{m^2} \langle \vec{L} \cdot \vec{S} \rangle e^{-\frac{10}{9}\beta^2 r^2} & \text{lin. (transfer)} \\ -\frac{5^{5/2}}{2^{1/2} 7^{5/2} \pi^{1/2}} \frac{b\beta}{m^2} \langle \vec{L} \cdot \vec{S} \rangle e^{-\frac{15}{14}\beta^2 r^2} & \text{lin. (capture)} \end{cases} \quad (29)$$

The OGE, linear and total spin-orbit potentials for the 3P_2 wave of $I=2$ $\pi\rho$ are shown in Fig.10 for our standard parameter set. The largest contribution to the $\pi\rho$ spin-orbit force comes from OGE transfer diagrams; the linear confinement spin-orbit from the transfer diagrams is about half as large and opposite in sign, and the two capture diagram contributions are much smaller. Since the confinement capture and transfer diagrams have opposite signs, the net result is dominance of the PsV spin-orbit by the OGE contribution.

D. Scattering in J^{PC_n} -Exotic PsV Channels.

TABLE I. J^{PC_n} Exotic States in PsV.

Channel		Exotic Quantum Numbers				
Meson Pair	I_{tot}	S	P	D	F	G
$\pi\rho$	0, 2	–	0^{--}	2^{+-}	–	4^{+-}
	1	–	1^{-+}	–	3^{-+}	
$\pi\omega, \eta\rho$	1	–	0^{--}	2^{+-}	–	4^{+-}
$\eta\omega$	0	–	0^{--}	2^{+-}	–	4^{+-}

The recent evidence for J^{PC_n} -exotic resonances $\pi_1(1400)$ and $\pi_1(1600)$ [35] has made the study of scattering amplitudes in exotic channels especially interesting. The surprisingly low mass of the $\pi_1(1400)$ in particular has led to suggestions that it might not be a “hybrid” gluonic excitation, since these are expected at $\approx 1.8 - 2.0$ GeV [36]. Another possibility that the $\pi_1(1400)$ is a “multiquark”, perhaps a meson-meson bound state in a very attractive channel. We can test the plausibility of this type of assignment by

calculating meson-meson scattering amplitudes in the various exotic channels.

The exotic channels accessible to the lightest nonstrange PsV meson pairs are listed in Table I. (We do not tabulate light PsPs exotic amplitudes because they are zero in this model. The PsPs exotic channels are odd- l $\pi\eta$, $\pi\eta'$ and $\eta\eta'$, whereas the quark interchange model PsPs scattering amplitudes are even- l , assuming identical spatial wavefunctions.) We generally expect the largest scattering amplitudes to be in the lower partial waves. In PsV the P-wave has the first exotics, which are $J^{PC_n} = 0^{--}$ (all channels except I=1 $\pi\rho$) and $J^{PC_n} = 1^{-+}$ (I=1 $\pi\rho$ only). Calculation of these scattering amplitudes simply requires changing the external $q\bar{q}$ flavor states attached to the Feynman diagrams of Fig.1. The results relative to the I=2 $\pi\rho$ case treated in the paper are summarized in Table II.

TABLE II. Overall flavor factors in diagonal PsV scattering.

Channel		Relative Amplitude
$\pi\rho$	I=2	+1
	1	0
	0	-1/2
$\pi\omega$	1	+1/2
$\eta\rho$	1	+1/4
$\eta\omega$	0	+1/4

Inspection of the tables shows that the largest exotic scattering amplitude should be in the I=2 $\pi\rho$ 0^{--} P-wave. The elastic phase shift in this channel is the 3P_0 curve in Fig.8. The large negative phase shift shows that this is a strongly repulsive channel; the maximum phase shift is predicted to be a quite large $\approx -50^\circ$ at $M_{\pi\rho} \approx 3.1$ GeV, which exceeds even the S-wave phase shift maximum. The largest *attractive* exotic phase shift we have found in PsV is the I=0 partner, which is $-1/2$ of I=2, giving a maximum phase shift of $\approx +25^\circ$ at the same mass. We do not find sufficient attraction to form a meson-meson “molecular” bound state in any of these nonstrange J^{PC_n} -exotic PsV channels.

The η channels are relatively weak because only the $n\bar{n}$ part of the η contributes to these diagonal scattering amplitudes; the $s\bar{s}$ component leads to open-strange final states ($K^*\bar{K}$ for example) after quark line interchange.

Regarding candidate exotic resonances, there have been speculations that the determination of the mass and width of the exotic candidate $\pi_1(1400)$ may have been compromised by inelastic rescattering effects [37], analogous to the ‘‘Deck effect’’ proposed as a nonresonant explanation of the $a_1(1260)$. For example, crossing the πb_1 threshold at ≈ 1.4 GeV in the process $\pi\rho \rightarrow \pi b_1 \rightarrow \pi\eta$ might mimic resonant phase motion if this process has a rapidly varying inelasticity. We can test this and other nonresonant possibilities by calculating the elementary $2 \rightarrow 2$ scattering amplitudes using our quark model approach.

Some important results follow from simple flavor factors. Note in particular that the nonresonant scattering amplitude $\pi\rho \rightarrow \pi\rho$ vanishes in any $I=1$ channel, including the π_1 exotic one. This is a general result whenever the quark line diagram of Fig.1 dominates; clearly a pair of oppositely charged, nonstrange $q\bar{q}$ mesons A^+B^- cannot scatter into another charged pair C^+D^- under quark interchange. A comparison with isospin matrix elements shows that this implies that scattering of any two $q\bar{q}$ isovectors in $I=1$ vanishes. This isospin selection rule eliminates two subprocesses discussed by Donnachie and Page [37] as Deck effect backgrounds that might shift a higher-mass exotic resonance to an apparent $\pi_1(1400)$, $\pi\rho \rightarrow \pi b_1 \rightarrow \pi\eta$ and $\pi\rho \rightarrow \pi\rho \rightarrow \pi\eta$.

Independent of any scattering model, one should note that the coupling $\pi\rho \rightarrow \pi b_1$ is probably small because of the strong VES experimental limit (reported by V.Dorofeev [35]) of

$$B(\pi_2(1670) \rightarrow \pi b_1) < 0.19\% \quad (2\sigma \text{ c.l.}) . \quad (30)$$

Since $\pi_2 \rightarrow \pi\rho$ is a large mode ($B = 31(4)\%$ [39]), if $\pi\rho \rightarrow \pi b_1$ rescattering were important we would also expect to observe a large $\pi_2 \rightarrow \pi b_1$ branching fraction.

We also expect the final background process suggested by Donnachie and Page ($\pi\rho \rightarrow \pi\eta \rightarrow \pi\eta$) to be small, because the direct time ordering $\pi\eta \rightarrow \pi\eta$ vanishes in P-wave in

this model. Finally, the rescattering process they propose, $\pi_1(1600) \rightarrow \pi b_1 \rightarrow \eta\pi$, does not vanish in the quark interchange model, although the required $\Delta l = 1$ and suppressed η flavor factor may nonetheless make this a relatively weak amplitude. A calculation of this and related scattering amplitudes is planned for a future publication.

E. Experimental prospects for measuring PsV phase shifts.

Although there is little experimental information about PsV interactions at present, these phase shifts actually are experimentally accessible in existing data, for example as relative FSI phases in the D and S amplitudes in $b_1 \rightarrow \omega\pi$. These are usually, and incorrectly, taken to be relatively real amplitudes. The relative phase including the FSI is $D/S = |D/S| \cdot e^{i(\delta_D - \delta_S)}$ [38], and is observable for example as a reduction in the strength of the SD cross term in the $\pi\omega$ angular distribution by $\cos(\delta_S - \delta_D)$. Since this method requires individual measurements of the S^2 , D^2 and SD cross term in the angular distribution, it should be applicable to cases such as $b_1(1230) \rightarrow \pi\omega$ and $b_1(1600) \rightarrow \pi\omega$ where S and D are of comparable magnitude [40]. The $\delta_{SD} = \delta_S - \delta_D$ phases we predict at these masses (which are calculated from +1/2 times the 3S_1 and 3D_1 I=2 $\pi\rho$ phases in Figs.7,8) are $\delta_{SD}^{\pi\omega}(M_{\pi\omega} = 1.23 \text{ GeV}) = -14.^{\circ}$ and $\delta_{SD}^{\pi\omega}(M_{\pi\omega} = 1.60 \text{ GeV}) = -17.^{\circ}$.

This proposed technique is similar to that used in K_{e4} decays [27], in which the low energy I=0 $\pi\pi$ S-wave phase shift is actually observed as the difference between the I=0 S-wave and I=1 P-wave $\pi\pi$ FSI phases.

III. SUMMARY AND CONCLUSIONS

In this paper we have derived meson-meson scattering amplitudes, including spin-dependent forces, from a calculation of the Born-order matrix element of the quark-quark interaction between two-meson states. Since $q\bar{q}$ annihilation is not included in the model, it describes scattering that does not involve coupling to s -channel resonances.

This includes for example $I=2$ and the nonresonant backgrounds in all channels, including exotic J^{PC_n} .

We considered the cases of PsPs and PsV scattering, and derived the scattering amplitudes in all j, l, s channels for these cases. The parameters of the model were previously fixed by quark model studies of hadron spectroscopy. Where possible we have compared the results to experiment.

In $I=2 \pi\pi$ (the best studied PsPs case) the results were shown to be in reasonable agreement with experiment in S-wave scattering, and an extremum predicted near $M_{\pi\pi} = 1.5$ GeV is supported by the data. Rapid variation of δ_0/k_π is predicted near threshold, which may reconcile theoretical expectations of a small scattering length with larger reported experimental values based on extrapolation in k_π^2 . The experimental D-wave, although quite small, is clearly larger than the model predicts.

The PsV system is a convenient theoretical laboratory for studying spin-dependent forces, since it can accommodate both spin-orbit and tensor interactions, and is simpler than KN or NN. We derived analytical results for these spin-dependent PsV interactions (T-matrices and phase shifts) given SHO wavefunctions and the standard spin-dependent quark model forces. The quark-quark spin-orbit and tensor forces map directly into spin-orbit and tensor PsV interactions. We find that the OGE spin-orbit force in the PsV system is quite large in P-wave, and so is expected to be large in many other hadron-hadron systems as well.

There is no PsV phase shift data at present. We noted however that PsV phase shifts actually can be measured in multi-amplitude resonance decays to PsV final states, so it should be possible to test theoretical predictions for PsV scattering amplitudes in future experimental studies.

Our predictions for scattering in J^{PC_n} -exotic channels are of current interest because the reported exotics might be complicated by large and rapidly varying nonresonant inelasticities. One speculation is that the $\pi_1(1400)$ parameters might be strongly affected

by the opening of inelastic couplings to the πb_1 channel. In our model (and in any $q\bar{q}$ constituent interchange model) several of these nonresonant processes can be rejected as significant complications because of vanishing flavor factors.

In future we plan to extend our calculations to other exotic meson-meson channels, such as S+P, to test whether strong attractive interactions are predicted that might support “multiquark exotics” such as S+P molecules. We also plan to apply the current approach to the study of spin-dependent interactions in other hadronic systems, including KN, NN and light hadron + charmonium systems.

IV. ACKNOWLEDGEMENTS

We are grateful to our colleagues D.Blaschke, N.Cason, H.G.Dosch, S.Krewald, E.Klempt, N.Isgur, C.Michael, M.R.Pennington, B.Pick, H.-J.Pirner, G.Röpke, F.Sassen, J.Speth, Fl.Stancu and C.-Y.Wong for useful discussions of various issues relating to meson-meson scattering.

This research was supported in part by the DOE Division of Nuclear Physics, at ORNL, managed by UT-Battelle, LLC, for the US Department of Energy under Contract No. DE-AC05-00OR22725. ES acknowledges support from the DOE under grant DE-FG02-96ER40944 and DOE contract DE-AC05-84ER40150 under which the Southeastern Universities Research Association operates the Thomas Jefferson National Accelerator Facility. TB acknowledges additional support from the Deutsche Forschungsgemeinschaft DFG at the University of Bonn and the Forschungszentrum Jülich under contract Bo 56/153-1.

APPENDIX A: QUARK-LEVEL T-MATRICES AND WAVEFUNCTIONS

The various contributions to the quark-quark T_{fi} (with color factors of $T^a T^a$ removed) are

$$T_{fi}(\vec{q}, \vec{p}_1, \vec{p}_2) = \begin{cases} -\frac{8\pi\alpha_s}{3m^2} \left[\vec{S}_1 \cdot \vec{S}_2 \right] & \text{OGE spin-spin} \\ +\frac{4\pi\alpha_s}{\vec{q}^2} & \text{OGE color Coulomb} \\ +\frac{6\pi b}{\vec{q}^4} & \text{linear conf.} \\ +\frac{4i\pi\alpha_s}{m^2\vec{q}^2} \left[\vec{S}_1 \cdot \left(\vec{q} \times \left(\frac{\vec{p}_1}{2} - \vec{p}_2 \right) \right) + \vec{S}_2 \cdot \left(\vec{q} \times \left(\vec{p}_1 - \frac{\vec{p}_2}{2} \right) \right) \right] & \text{OGE spin-orbit} \\ -\frac{3i\pi b}{m^2\vec{q}^4} \left[\vec{S}_1 \cdot (\vec{q} \times \vec{p}_1) - \vec{S}_2 \cdot (\vec{q} \times \vec{p}_2) \right] & \text{linear spin-orbit} \\ +\frac{4\pi\alpha_s}{m^2\vec{q}^2} \left[\vec{S}_1 \cdot \vec{q} \vec{S}_2 \cdot \vec{q} - \frac{1}{3} \vec{q}^2 \vec{S}_1 \cdot \vec{S}_2 \right] & \text{OGE tensor.} \end{cases} \quad (\text{A1})$$

The standard $q\bar{q}$ quark model Gaussian wavefunction is given by

$$\Phi(\vec{p}_{rel}) = \frac{1}{\pi^{3/4} \beta^{3/2}} e^{-\vec{p}_{rel}^2/8\beta^2} \quad (\text{A2})$$

where in general

$$\vec{p}_{rel} = \frac{m_{\bar{q}}\vec{p}_q - m_q\vec{p}_{\bar{q}}}{(m_q + m_{\bar{q}})/2} \quad (\text{A3})$$

and for our special case of equal quark and antiquark masses

$$\vec{p}_{rel} = \vec{p}_q - \vec{p}_{\bar{q}}. \quad (\text{A4})$$

APPENDIX B: EXPLICIT OVERLAP INTEGRALS

B1. Results Included

In this appendix we give the explicit meson-meson T-matrix elements that follow from the overlap integrals Eqs.(1-4) with Gaussian wavefunctions and the various quark T-matrix elements. The OGE spin-spin hyperfine, color Coulomb and linear confinement results were derived previously [13]. For completeness we quote the formulas here, as well as giving the new spin-orbit and tensor results. The multiplicative diagram-dependent color and flavor factors and the signature phase (which is (-1) for these meson-meson scattering diagrams) are not included in the results given below. These formulas abbreviate the confluent hypergeometric function ${}_1F_1(a; c; x)$ as $f_{a,c}(x)$, and $\vec{Q}_\pm = (\vec{C} \pm \vec{A})$.

B2. OGE Spin-Spin Hyperfine Contribution

These simple contact matrix elements were evaluated previously, for example in Ref. [9] (in an equivalent form, but incorporating color factors and the signature phase, as Eqs.(71-73) of that reference). The results are

$$T_{fi}^{(T1)} = -\frac{2^3}{3} \frac{\pi\alpha_s}{m^2} e^{-\vec{Q}_+^2/8\beta^2} [\vec{S}_1 \cdot \vec{S}_2] \quad (B1)$$

$$T_{fi}^{(T2)} = T_{fi}^{(T1)}(\vec{C} \rightarrow -\vec{C}) \quad (B2)$$

$$T_{fi}^{(C1)} = -\frac{2^6}{3^{5/2}} \frac{\pi\alpha_s}{m^2} e^{-\vec{A}^2/3\beta^2} [\vec{S}_1 \cdot \vec{S}_2] \quad (B3)$$

$$T_{fi}^{(C2)} = T_{fi}^{(C1)} . \quad (B4)$$

B3. OGE Color Coulomb Contribution

The contribution of the OGE color Coulomb interaction to the meson-meson T-matrix follows from the evaluation of the integrals Eqs.(1-4) with the second quark-quark T_{fi} in Eq.(A1). The results are

$$T_{fi}^{(T1)} = + 2^2 \frac{\pi\alpha_s}{\beta^2} f_{\frac{1}{2}, \frac{3}{2}}(\vec{Q}_-^2/8\beta^2) e^{-\vec{A}^2/2\beta^2} \quad (\text{B5})$$

$$T_{fi}^{(T2)} = T_{fi}^{(T1)}(\vec{C} \rightarrow -\vec{C}) \quad (\text{B6})$$

$$T_{fi}^{(C1)} = + \frac{2^3}{3^{1/2}} \frac{\pi\alpha_s}{\beta^2} f_{\frac{1}{2}, \frac{3}{2}}(\vec{A}^2/6\beta^2) e^{-\vec{A}^2/2\beta^2} \quad (\text{B7})$$

$$T_{fi}^{(C2)} = T_{fi}^{(C1)} . \quad (\text{B8})$$

B4. Linear Confinement Contribution

The linear confinement integrals were carried out in coordinate space, since the Fourier transform of the linear potential is singular. The results are

$$T_{fi}^{(T1)} = -6 \frac{\pi b}{\beta^4} f_{-\frac{1}{2}, \frac{3}{2}}(\vec{Q}_-^2/8\beta^2) e^{-\vec{A}^2/2\beta^2} \quad (\text{B9})$$

$$T_{fi}^{(T2)} = T_{fi}^{(T1)}(\vec{C} \rightarrow -\vec{C}) \quad (\text{B10})$$

$$T_{fi}^{(C1)} = - 3^{3/2} \frac{\pi b}{\beta^4} f_{-\frac{1}{2}, \frac{3}{2}}(\vec{A}^2/6\beta^2) e^{-\vec{A}^2/2\beta^2} \quad (\text{B11})$$

$$T_{fi}^{(C2)} = T_{fi}^{(C1)} . \quad (\text{B12})$$

One may also obtain these results using the momentum space integrals Eqs.(1-4), but the $1/q^4$ quark-quark T_{fi} in Eq.(A1) must include a long-distance regularization in the intermediate stages of the integration. The final result is well defined due to the Gaussian damping provided by the wavefunctions. We have checked both the linear and color Coulomb T_{fi} results by comparing the expressions Eqs.(B5-B12) with Monte Carlo evaluations of the corresponding real-space overlap integrals.

B5. OGE Spin-Orbit Contribution

The four OGE spin-orbit overlap integrals can be evaluated similarly using the fourth quark-quark T_{fi} in Eq.(A1), which gives

$$T_{fi}^{(\text{T1})} = -\frac{\pi\alpha_s}{m^2\beta^2} f_{\frac{3}{2},\frac{5}{2}}(\vec{Q}_-^2/8\beta^2) e^{-\vec{A}^2/2\beta^2} \left[(\vec{S}_1 + \vec{S}_2) \cdot i(\vec{A} \times \vec{C}) \right] \quad (\text{B13})$$

$$T_{fi}^{(\text{T2})} = T_{fi}^{(\text{T1})}(\vec{C} \rightarrow -\vec{C}) \quad (\text{B14})$$

$$T_{fi}^{(\text{C1})} = +\frac{4}{3^{5/2}} \frac{\pi\alpha_s}{m^2\beta^2} f_{\frac{3}{2},\frac{5}{2}}(\vec{A}^2/6\beta^2) e^{-\vec{A}^2/2\beta^2} \left[(\vec{S}_1 - \vec{S}_2) \cdot i(\vec{A} \times \vec{C}) \right] \quad (\text{B15})$$

$$T_{fi}^{(\text{C2})} = -T_{fi}^{(\text{C1})} . \quad (\text{B16})$$

B6. Scalar Confinement Spin-Orbit Contribution

The matrix elements Eqs.(1-4), of the scalar confinement spin-orbit interaction in Eq.(A1) are

$$T_{fi}^{(\text{T1})} = +\frac{1}{2} \frac{\pi b}{m^2\beta^4} f_{\frac{1}{2},\frac{5}{2}}(\vec{Q}_-^2/8\beta^2) e^{-\vec{A}^2/2\beta^2} \left[(\vec{S}_1 + \vec{S}_2) \cdot i(\vec{A} \times \vec{C}) \right] \quad (\text{B17})$$

$$T_{fi}^{(\text{T2})} = T_{fi}^{(\text{T1})}(\vec{C} \rightarrow -\vec{C}) \quad (\text{B18})$$

$$T_{fi}^{(\text{C1})} = +\frac{1}{2 \cdot 3^{1/2}} \frac{\pi b}{m^2\beta^4} f_{\frac{1}{2},\frac{5}{2}}(\vec{A}^2/6\beta^2) e^{-\vec{A}^2/2\beta^2} \left[(\vec{S}_1 - \vec{S}_2) \cdot i(\vec{A} \times \vec{C}) \right] \quad (\text{B19})$$

$$T_{fi}^{(\text{C2})} = -T_{fi}^{(\text{C1})} . \quad (\text{B20})$$

B7. OGE Tensor Contribution

Finally, for the OGE tensor T_{fi} (the last entry in Eq.(A1) we find

$$T_{fi}^{(\text{T1})} = +\frac{1}{5} \frac{\pi\alpha_s}{m^2\beta^2} f_{\frac{5}{2},\frac{7}{2}}(\vec{Q}_-^2/8\beta^2) e^{-\vec{A}^2/2\beta^2} \left[\vec{S}_1 \cdot \vec{Q}_- \vec{S}_2 \cdot \vec{Q}_- - \frac{1}{3} \vec{Q}_-^2 \vec{S}_1 \cdot \vec{S}_2 \right] \quad (\text{B21})$$

$$T_{fi}^{(\text{T2})} = T_{fi}^{(\text{T1})}(\vec{C} \rightarrow -\vec{C}) \quad (\text{B22})$$

$$T_{fi}^{(\text{C1})} = +\frac{2^5}{3^{5/2} \cdot 5} \frac{\pi\alpha_s}{m^2\beta^2} f_{\frac{5}{2},\frac{7}{2}}(\vec{A}^2/6\beta^2) e^{-\vec{A}^2/2\beta^2} \left[\vec{S}_1 \cdot \vec{A} \vec{S}_2 \cdot \vec{A} - \frac{1}{3} \vec{A}^2 \vec{S}_1 \cdot \vec{S}_2 \right] \quad (\text{B23})$$

$$T_{fi}^{(\text{C2})} = T_{fi}^{(\text{C1})} . \quad (\text{B24})$$

The tensor matrix elements in the capture diagrams, Eqs.(B23,B24), are the only cases in which we have found a post-prior discrepancy in these PsPs and PsV scattering amplitudes; the post forms of these matrix elements involve a tensor in \vec{C} rather than \vec{A} ,

$$T_{fi}^{(C1,\text{post})} = + \frac{2^5}{3^{5/2} \cdot 5} \frac{\pi\alpha_s}{m^2\beta^2} f_{\frac{5}{2},\frac{7}{2}}(\vec{A}^2/6\beta^2) e^{-\vec{A}^2/2\beta^2} \left[\vec{S}_1 \cdot \vec{C} \vec{S}_2 \cdot \vec{C} - \frac{1}{3} \vec{C}^2 \vec{S}_1 \cdot \vec{S}_2 \right].$$

(B25)

These capture tensor terms vanish in the PsPs channel. They do make a small, off-diagonal contribution to PsV scattering, *albeit* only in the ${}^3S_1 \leftrightarrow {}^3D_1$ amplitude.

APPENDIX C: MAPPING QUARK SPINS INTO HADRON SPINS.

C1. Spin Matrix Elements

In these scattering amplitude calculations the matrix elements of spin-dependent quark interactions (the spin-spin, spin-orbit and tensor forces) involve matrix elements of linear and bilinear quark spin operators. Since the quark spins are not directly observed, it is useful to replace them by the spins of the external hadrons. This appendix gives the (diagram dependent) mapping from quark spins to hadron spins in the PsPs and PsV cases considered in this paper.

The spin matrix elements we require are I , $S(1)^i$, $S(2)^i$ and $S(1)^i S(2)^j$ between general initial and final PsPs and PsV spin states. Our convention for the diagrams (Fig.1) is that mesons A and C are always Ps (*e.g.* π), and B and D are Ps or V (*e.g.* π or ρ).

C2. PsPs

First, in PsPs scattering there are no external meson spins, so the quark spin matrix elements are proportional to geometrical tensors such as δ^{ij} . The matrix elements by diagram are

$$\langle PsPs | I | PsPs \rangle = +\frac{1}{2} \quad \text{all diagrams} \quad (C1)$$

$$\langle PsPs | S(1)^i | PsPs \rangle = \langle PsPs | S(2)^i | PsPs \rangle = 0 \quad \text{all diagrams} \quad (C2)$$

$$\langle PsPs | S(1)^i S(2)^j | PsPs \rangle = \begin{cases} +\frac{1}{8} \delta^{ij} & \text{T1, T2, T1}_{symm}, \text{T2}_{symm} \\ -\frac{1}{8} \delta^{ij} & \text{C1, C2, C1}_{symm}, \text{C2}_{symm} \end{cases} \quad \text{hence} \quad (C3)$$

$$\langle PsPs | \vec{S}(1) \cdot \vec{S}(2) | PsPs \rangle = \begin{cases} +\frac{3}{8} & \text{T1, T2, T1}_{symm}, \text{T2}_{symm} \\ -\frac{3}{8} & \text{C1, C2, C1}_{symm}, \text{C2}_{symm} \end{cases} . \quad (C4)$$

Note that the spin-orbit and tensor terms vanish identically in PsPs scattering; this follows from applying Eqs.(C2,C3) to Eq.(A1).

C3. PsV

In PsV scattering the vector (*e.g.* ρ) meson spin \vec{S}_ρ provides an additional degree of freedom, and the linear and quadratic quark spin matrix elements can be expressed in terms of the ρ spin matrix elements $\langle \rho_f | S_\rho^i | \rho_i \rangle$ and $\langle \rho_f | S_\rho^i S_\rho^j | \rho_i \rangle$. The mapping of quark to meson spins is

$$\langle (\pi\rho)_f | I | (\pi\rho)_i \rangle = +\frac{1}{2} \langle \rho_f | I | \rho_i \rangle \quad \text{all diagrams} \quad (\text{C5})$$

$$\langle (\pi\rho)_f | S(1)^i | (\pi\rho)_i \rangle = \begin{cases} -\frac{1}{4} \langle \rho_f | S_\rho^i | \rho_i \rangle & \text{T1, T2}_{symm}, \text{C1, C2}_{symm} \\ +\frac{1}{4} \langle \rho_f | S_\rho^i | \rho_i \rangle & \text{T2, T1}_{symm}, \text{C2, C1}_{symm} \end{cases} \quad (\text{C6})$$

$$\langle (\pi\rho)_f | S(2)^i | (\pi\rho)_i \rangle = +\frac{1}{4} \langle \rho_f | S_\rho^i | \rho_i \rangle \quad \text{all diagrams} \quad (\text{C7})$$

$$\langle (\pi\rho)_f | S(1)^i S(2)^j | (\pi\rho)_i \rangle = \begin{cases} +\frac{1}{8} \delta^{ij} \langle \rho_f | I | \rho_i \rangle + \frac{1}{8} i \epsilon^{ijk} \langle \rho_f | S_\rho^k | \rho_i \rangle - \frac{1}{4} \langle \rho_f | S_\rho^i S_\rho^j | \rho_i \rangle & \text{T1, T2}_{symm} \\ +\frac{1}{8} \delta^{ij} \langle \rho_f | I | \rho_i \rangle + \frac{1}{8} i \epsilon^{ijk} \langle \rho_f | S_\rho^k | \rho_i \rangle & \text{T2, T1}_{symm} \\ -\frac{1}{8} \delta^{ij} \langle \rho_f | I | \rho_i \rangle - \frac{1}{8} i \epsilon^{ijk} \langle \rho_f | S_\rho^k | \rho_i \rangle & \text{C1, C2}_{symm} \\ -\frac{1}{8} \delta^{ij} \langle \rho_f | I | \rho_i \rangle - \frac{1}{8} i \epsilon^{ijk} \langle \rho_f | S_\rho^k | \rho_i \rangle + \frac{1}{4} \langle \rho_f | S_\rho^i S_\rho^j | \rho_i \rangle & \text{C2, C1}_{symm} \end{cases} \quad (\text{C8})$$

**APPENDIX D: PHASE SHIFTS AND INELASTICITIES FROM THE
T-MATRIX**

Since total angular momentum is conserved, the T-matrix is block diagonal in a total angular momentum basis, and can be written as

$$T = \sum_{jm} |jm\rangle T_j \langle jm| . \quad (D1)$$

The coefficients $\{T_j\}$ can be determined by evaluating the matrix element

$$T_j = \langle jm| T |jm\rangle . \quad (D2)$$

In the special case of spinless scattering these basis states are eigenstates of orbital angular momentum

$$|lm\rangle = \int d\Omega Y_{lm}(\Omega) |\Omega\rangle , \quad (D3)$$

so the T-matrix is given by

$$T = \sum_{lm} |lm\rangle T_l \langle lm| = \sum_{lm} \iint d\Omega d\Omega' |\Omega'\rangle Y_{lm}(\Omega') T_l Y_{lm}^*(\Omega) \langle\Omega| . \quad (D4)$$

The T-matrix can also be written in terms of the scattering amplitude $T_{fi}(\Omega, \Omega')$ between momentum eigenstates,

$$T = \iint d\Omega d\Omega' |\Omega'\rangle T_{fi}(\Omega, \Omega') \langle\Omega| , \quad (D5)$$

so $T_{fi}(\Omega, \Omega')$ and T_l are related by

$$T_{fi}(\Omega, \Omega') = \sum_l T_l \sum_m Y_{lm}(\Omega') Y_{lm}^*(\Omega) = \sum_l \frac{2l+1}{4\pi} T_l P_l(\mu) \quad (D6)$$

and hence

$$T_l = \langle lm| T |lm\rangle = \iint d\Omega d\Omega' Y_{lm}^*(\Omega') T_{fi}(\Omega, \Omega') Y_{lm}(\Omega) \quad (D7)$$

where $\mu = \cos \theta_{\Omega\Omega'}$. A more familiar quantum-mechanical result follows from fixing the incident direction $\Omega = \hat{z}$ in Eq.(D6) and integrating over final angles with a $P_l(\mu)$ weight, which gives

$$T_l = 2\pi \int_{-1}^1 d\mu P_l(\mu) T_{fi}(\hat{z}, \Omega') . \quad (\text{D8})$$

Since we define $T_{fi}(\Omega, \Omega')$ by

$$\langle C_{\Omega'}, D_{-\Omega'} | S | A_{\Omega}, B_{-\Omega} \rangle = \delta_{fi} - i (2\pi)^4 \delta^{(4)}(A + B - C - D) T_{fi} , \quad (\text{D9})$$

it is related to the Lorentz invariant $2 \rightarrow 2$ scattering amplitude \mathcal{M} defined by the PDG [39] (their Eq.(35.8)) by

$$T_{fi} = \frac{\mathcal{M}}{\prod_{n=1}^4 (2E_n)^{1/2}} \quad (\text{D10})$$

and hence to the CM scattering amplitude $f(k, \theta)$ (their Eq.(35.48)) by

$$T_{fi} = -\frac{8\pi}{\sqrt{s}} f(k, \theta) . \quad (\text{D11})$$

(Here k is the CM momentum of any particle, $k = |\vec{A}| = |\vec{B}| = |\vec{C}| = |\vec{D}|$.) The partial wave expansion of $f(k, \theta)$, Eq.(35.44),

$$f(k, \theta) = \sum_l (2l + 1) a_l P_l(\mu) \quad (\text{D12})$$

and the relation between a diagonal partial wave amplitude a_l and the phase shift

$$a_l = \frac{e^{2i\delta_l} - 1}{2i} \quad (\text{D13})$$

allow us to determine δ_l from T_{fi} . For purely elastic scattering, and assuming small phase shifts so that $a_l \approx \delta_l$, Eqs.(D6-D13) give

$$\delta_l = -\frac{1}{4\pi} \frac{kE_A E_B}{\sqrt{s}} \int d\mu P_l(\mu) T_{fi}(\hat{z}, \Omega') = -\frac{1}{8\pi^2} \frac{kE_A E_B}{\sqrt{s}} T_l . \quad (\text{D14})$$

This relation was used previously to determine for example $K\pi$ [11] and l -diagonal KN [12] elastic phase shifts. In the case of elastic scattering of identical bosons, such as $I=2 \pi\pi$, there is an additional factor of two for identical particles [38], so the relation between the Born-order phase shift and the T-matrix element becomes

$$\delta_l \Big|_{ident.} = -\frac{kE_A}{16\pi} \int_{-1}^{+1} T_{fi} P_l(\mu) d\mu . \quad (\text{D15})$$

Since the angular integral in Eq.(D14) is proportional to the amplitude $\langle lm|T|lm\rangle$, we may also write the Born-order elastic phase shift (for distinguishable particles) directly in terms of the T-matrix,

$$\delta_l = -\frac{1}{8\pi^2} \frac{kE_A E_B}{\sqrt{s}} \langle lm|T|lm\rangle . \quad (\text{D16})$$

This formula has a straightforward generalization to the case of external hadrons with spin, which we use to evaluate $\pi\rho$ phase shifts and inelasticities. In the case of an l - and s -diagonal interaction this is

$$\delta_{jls} = -\frac{1}{8\pi^2} \frac{kE_A E_B}{\sqrt{s}} \langle jm; ls|T|jm; ls\rangle . \quad (\text{D17})$$

This is adequate for diagonal forces such as our $\pi\rho$ spin-orbit interactions. The tensor force however is not l -diagonal, so for this case we must introduce a more general parametrization. Since the tensor interaction couples l, l' channel pairs which have the same j but differ by $|l - l'| = 2$, it leads to 2×2 \mathcal{S} -matrices. These can be parametrized as

$$\mathcal{S}^j = \begin{bmatrix} \eta_W e^{2i\delta_l} & i\sqrt{1 - \eta_{W'}^2} e^{i(\delta_l + \delta_{l'})} \\ i\sqrt{1 - \eta_{W'}^2} e^{i(\delta_l + \delta_{l'})} & \eta_W e^{2i\delta_{l'}} \end{bmatrix} . \quad (\text{D18})$$

In our calculation, both of the phase shifts and the inelasticity $\epsilon_{W'} \equiv \sqrt{1 - \eta_{W'}^2}$ are $O(H_I)$, so to this order we can relate these linearly to the matrix elements of H_I . The Born order phase shift formula (D17) remains valid for both channels, and the inelasticity is

$$\epsilon_{W'} = -\frac{1}{4\pi^2} \frac{kE_A E_B}{\sqrt{s}} \langle jm; l's|T|jm; ls\rangle . \quad (\text{D19})$$

The overall phase of $\epsilon_{W'}$ is dependent on the state normalizations, but the familiar

$$\eta_W = \left| \sqrt{1 - \epsilon_{W'}^2} \right| \quad (\text{D20})$$

is unique.

APPENDIX E: POTENTIALS FROM THE T-MATRIX

Potentials provide a very useful representation of hadron-hadron interactions. They have a clear intuitive meaning, and can easily be used in the nonrelativistic Schrödinger equation in searches for bound states or in coupled channel problems.

Unfortunately, one may define hadron-hadron potentials in many different ways. Ideally they should reproduce phase shifts or T-matrix elements, at least in the low energy limit. The assumption of a unique, purely local potential is in general overly restrictive, as it leads to a scattering amplitude that is a function of t only. In general we find $2 \rightarrow 2$ scattering amplitudes that depend on both s and t . One approach to this problem is to introduce nonlocal “gradient” corrections to the potential [31], which can be expressed for example as $V(r) \vec{L} \cdot \vec{S}$ terms; this approach leads to the familiar Breit-Fermi Hamiltonian for one-photon and one-gluon exchange, and was used to define hadron-hadron potentials in our previous work [9,13].

Alternatively one may project the scattering amplitude onto a given angular channel l so that only s dependence remains, and find a local l -wave potential that describes the scattering in that channel. This definition of potentials was discussed by Mott and Massey [30], and is equivalent to the definition we shall use here. This approach was previously used by Swanson [10] to define meson-meson potentials from scattering amplitudes.

The quantum mechanical relation between the phase shift $\delta_l(k)$ and the radial wavefunction $R_l(r)$ in potential scattering of a mass μ particle (which becomes the reduced mass below) in first Born approximation is

$$\delta_l = -2\mu k \int_0^\infty r^2 dr V(r) j_l(kr)^2 . \quad (\text{E1})$$

Since our T-matrix elements implicitly determine the elastic scattering phase shifts, for example the $I = 2 \pi\pi$ S-wave in Eq.(6), we can invert this formula for each l to determine the corresponding l -wave local potential $V_l(r)$. In practice we find that our phase shifts are sufficiently “hard” at high energies to require singular potentials; this is presumably

an artifact of our approximations, such as assuming a contact spin-spin interaction. For this reason we do not completely invert the phase shift relation (E1), and instead simply fit an assumed Gaussian form

$$V(r) = V_g e^{-r^2/r_g^2} \quad (\text{E2})$$

to our theoretical *low energy* phase shift. The two Gaussian parameters are determined from the $O(k)$ and $O(k^3)$ terms in the expansion of the phase shift near threshold, which in the S-wave case are equated to

$$\lim_{k \rightarrow 0} \delta_0(k) = -\frac{\pi^{1/2}}{2} \mu V_g r_g^3 k \left(1 - \frac{1}{2} r_g^2 k^2 + O(k^4) \right). \quad (\text{E3})$$

The generalization to higher l , also using Eqs.(E1), is

$$\lim_{k \rightarrow 0} \delta_l(k) = -\frac{\pi^{1/2}}{2} \mu V_g r_g^3 \frac{(r_g^2/2)^l}{(2l+1)!!} k^{2l+1} \left(1 - \frac{1}{2} r_g^2 k^2 + O(k^4) \right). \quad (\text{E4})$$

In determining the Gaussian potentials that correspond to our derived phase shifts such as Eqs.(6,14,28), we set the external factors of E_π and E_ρ equal to m_π and m_ρ before expanding in k . This corresponds to using nonrelativistic phase space and nonrelativistic external hadron line normalizations in our T-matrix calculations, which we assume is the appropriate choice for the derivation of a nonrelativistic equivalent potential.

APPENDIX F: THE POST-PRIOR DISCREPANCY

The “post-prior discrepancy” is a familiar problem in rearrangement collisions; the diagrams of Fig.1 treat the scattering as due to an interaction between the initial hadrons A and B (“prior”), but we could equally well have written the interaction between the two final hadrons C and D (“post”). The post T-matrices may be obtained from the prior ones by exchanging the initial and final mesons and transforming the momenta $\vec{A} \rightarrow \vec{C}$, $\vec{C} \rightarrow \vec{A}$ and $\vec{q} \rightarrow -\vec{q}$. Thus for example the post C1 T-matrix is

$$\begin{aligned}
 T_{fi}^{(C1,post)}(AB \rightarrow CD) &= \\
 &\iint d^3q d^3p \Phi_C^*(2\vec{p} + \vec{q} - \vec{C}) \Phi_D^*(2\vec{p} + \vec{q} - 2\vec{A} - \vec{C}) \\
 &T_{fi}(\vec{q}, \vec{p}, -\vec{p} + \vec{A}) \Phi_A(2\vec{p} - \vec{q} - \vec{A}) \Phi_B(2\vec{p} + \vec{q} - \vec{A} - 2\vec{C}) . \quad (F1)
 \end{aligned}$$

$$= T_{fi}^{(C1,prior)}(AB \rightarrow CD) \Big|_{\substack{(\Phi_A, \Phi_B, \Phi_C^*, \Phi_D^*) \rightarrow (\Phi_C^*, \Phi_D^*, \Phi_A, \Phi_B), \\ \text{args } \vec{A} \rightarrow \vec{C}, \vec{C} \rightarrow \vec{A}, \vec{q} \rightarrow -\vec{q}}} . \quad (F2)$$

One may show that the post and prior results for the scattering amplitude are equal provided that the external wavefunctions are eigenfunctions of the Hamiltonian [41]. Swanson [10] shows an example of convergence of post and prior results for meson-meson scattering amplitudes derived from quark Born diagrams as the external wavefunctions approach exact Hamiltonian eigenstates. Of course the Gaussian wavefunctions we use to derive our analytical results are only approximations to the eigenfunctions of the full OGE plus linear Hamiltonian, so in general we can expect to find a post-prior discrepancy. In this study we actually find such a discrepancy only in part of the tensor interaction in PsV scattering, for which we take the mean of the two results,

$$T_{fi}(AB \rightarrow CD) = \frac{1}{2} \left(T_{fi}^{post}(AB \rightarrow CD) + T_{fi}^{prior}(AB \rightarrow CD) \right) . \quad (F3)$$

APPENDIX G: Y_{LM} EXPANSIONS AND RELATED INTEGRALS

It is useful in the partial wave decomposition of scattering amplitudes to expand functions of the sum and difference momentum transfers $\vec{Q}_\pm = \vec{C} \pm \vec{A}$ (here $|\vec{A}| = |\vec{C}|$) in spherical harmonics,

$$f(\vec{Q}_+^2) = \sum_{\ell} f_{\ell}(\vec{A}^2) \sum_m Y_{\ell m}^*(\Omega_C) Y_{\ell m}(\Omega_A) , \quad (\text{G1})$$

$$f(\vec{Q}_-^2) = \sum_{\ell} (-1)^{\ell} f_{\ell}(\vec{A}^2) \sum_m Y_{\ell m}^*(\Omega_C) Y_{\ell m}(\Omega_A) . \quad (\text{G2})$$

This expansion may be inverted to determine the coefficient functions $\{f_{\ell}(\vec{A}^2)\}$,

$$\begin{aligned} f_{\ell}(\vec{A}^2) &= 2\pi \int_{-1}^1 d\mu P_{\ell}(\mu) f(\vec{Q}_+^2) \\ &= 2\pi \int_{-1}^1 d\mu P_{\ell}(\mu) f(2\vec{A}^2(1+\mu)) = 2\pi(-1)^{\ell} \int_{-1}^1 d\mu P_{\ell}(\mu) f(2\vec{A}^2(1-\mu)) . \end{aligned} \quad (\text{G3})$$

Many of the scattering amplitudes derived in this paper are proportional to confluent hypergeometric functions in \vec{Q}_+^2 or \vec{Q}_-^2 , and their partial wave decomposition requires the integral of a Legendre polynomial times a shifted confluent hypergeometric function. This integral is given by (abbreviating ${}_1F_1(a; c; x)$ as $f_{a,c}(x)$)

$$\mathcal{F}_{a,c}^{(\ell)}(x) = \int_{-1}^1 d\mu P_{\ell}(\mu) f_{a,c}(x(1+\mu)) = \sum_{m=0}^{\ell} c_m^{(\ell)} \frac{(a)_{-m-1}}{(c)_{-m-1}} \frac{(f_{a-m-1,c-m-1}(2x) + (-1)^{\ell+m+1})}{x^{m+1}} \quad (\text{G4})$$

where

$$c_m^{(\ell)} = \frac{(-1)^m}{2^m m!} \frac{(\ell+m)!}{(\ell-m)!} \quad (\text{G5})$$

and the Pochhammer symbol of negative index is

$$(a)_{-n} = \frac{\Gamma(a-n)}{\Gamma(a)} = \frac{1}{\prod_{k=1}^n (a-k)} . \quad (\text{G6})$$

In numerical evaluations it is often useful to transform the confluent hypergeometric function in Eq.(G4) to a more rapidly converging negative-argument form, using $f_{a,c}(2x) = f_{c-a,c}(-2x) e^{2x}$.

APPENDIX H: SPIN-ORBIT AND TENSOR MATRIX ELEMENTS

As noted in App.D, when evaluating phase shifts and inelasticities it is useful to determine T-matrix elements between $|jls\rangle$ states. In the PsV system there are spin-orbit and tensor contributions to the T-matrix, and determination of the j, l, s -basis matrix elements of these terms is a complicated problem in angular analysis. Here we show how these matrix elements may be evaluated.

First consider the spin-orbit terms in the $\pi\rho$ T-matrix, Eq.(16). The generic term is of the form

$$T_{fi} = f(\vec{Q}_+^2) [i\vec{S}_\rho \cdot (\vec{A} \times \vec{C})] , \quad (\text{H1})$$

where $\vec{Q}_+ = \vec{C} + \vec{A}$. (Additional dependence on the rotational scalar $\vec{A}^2 = \vec{C}^2$ is a trivial modification of this angular decomposition.) To proceed, we expand $f(\vec{Q}_+^2)$ in spherical harmonics, as in Eq.(G1);

$$f(\vec{Q}_+^2) = \sum_{\ell} f_{\ell}(\vec{A}^2) \sum_m Y_{\ell m}^*(\Omega_C) Y_{\ell m}(\Omega_A) \quad (\text{H2})$$

and introduce spherical components for the spin and momentum vectors,

$$\langle 1s'_z | S_\mu | 1s_z \rangle = -\sqrt{2} \langle 1s'_z | 1\mu, 1s_z \rangle , \quad (\text{H3})$$

$$i(\vec{A} \times \vec{C})_\mu = \frac{4\sqrt{2}\pi}{3} A^2 \sum_{\mu'\mu''} \langle 1\mu', 1\mu'' | 1\mu \rangle Y_{1\mu'}(\Omega_A) Y_{1\mu''}(\Omega_C) \quad (\text{H4})$$

and the usual state vector expansion,

$$|jm, ls (PsV)\rangle = \sum_{\mu, s_z} \langle l\mu, 1s_z | jm \rangle Y_{l\mu}(\Omega_A) |1s_z\rangle . \quad (\text{H5})$$

With these substitutions one may determine the $\pi\rho \langle jl's | T_{fi} | jls \rangle$ matrix elements (analogous to the spinless matrix element T_l of Eq.(D7)) for the spin-orbit term (H1). The result involves a sum over a product of six Clebsch-Gordon coefficients, and can be written as the product of two Wigner $\{3j\}$ symbols and two $\{6j\}$ symbols,

$$\langle j'l's|T_{fi}|jls\rangle = (-1)^{j+1}6\vec{A}^2 \sum_{\ell} (-1)^{\ell} f_{\ell} (2\ell + 1) \sqrt{(2\ell + 1)(2\ell' + 1)}$$

$$\cdot \begin{pmatrix} 1 & l & \ell \\ 0 & 0 & 0 \end{pmatrix} \begin{pmatrix} 1 & l' & \ell \\ 0 & 0 & 0 \end{pmatrix} \begin{Bmatrix} 1 & 1 & 1 \\ l & l' & \ell \end{Bmatrix} \begin{Bmatrix} 1 & 1 & 1 \\ l & l' & j \end{Bmatrix}. \quad (\text{H6})$$

The constraints of the $(3j)$ and $\{6j\}$ symbols force this matrix element to be diagonal in l, l' , and imply that the only radial components of $f(\vec{Q}_+^2)$ in Eq.(H2) that contribute are $f_{\ell=l\pm 1}$. Substitution of the explicit $(3j)$ and $\{6j\}$ symbols gives our final result for PsV matrix elements of spin-orbit (H1) type,

$$\langle j'l's|T_{fi}|jls\rangle = \delta_{l'l'} \frac{[j(j+1) - l(l+1) - 2]}{2(2l+1)} \vec{A}^2 (f_{l-1} - f_{l+1}). \quad (\text{H7})$$

This result has the overall $\langle \vec{L} \cdot \vec{S} \rangle$ dependence that one would expect from a spin-orbit force.

We may similarly evaluate the matrix elements of the tensor terms in Eq.(16). It suffices to consider the two cases

$$T_{fi}^{(t1)} = f(\vec{Q}_-^2) \left([\vec{S}_{\rho} \cdot \vec{A} \vec{S}_{\rho} \cdot \vec{A} - \frac{2}{3}\vec{A}^2] + [\vec{S}_{\rho} \cdot \vec{C} \vec{S}_{\rho} \cdot \vec{C} - \frac{2}{3}\vec{C}^2] \right) \quad (\text{H8})$$

and

$$T_{fi}^{(t2)} = f(\vec{Q}_-^2) [\vec{S}_{\rho} \cdot \vec{A} \vec{S}_{\rho} \cdot \vec{C} - \frac{2}{3}\vec{A} \cdot \vec{C}]. \quad (\text{H9})$$

Both tensor matrix elements have $l \neq l'$ contributions, unlike the other interactions we have considered. The general results in terms of Wigner $(3j)$ and $\{6j\}$ symbols are

$$\langle j'l's|T_{fi}^{(t1)}|jls\rangle = (-1)^{j+l+1} \frac{2^{1/2} \cdot 5^{1/2}}{3^{1/2}} \vec{A}^2 (f_l + f_{l'}) \sqrt{(2l+1)(2l'+1)}$$

$$\cdot \begin{pmatrix} 2 & l & l' \\ 0 & 0 & 0 \end{pmatrix} \begin{Bmatrix} 1 & 1 & 2 \\ l & l' & j \end{Bmatrix} \quad (\text{H10})$$

and

$$\begin{aligned}
\langle j'l's|T_{f_i}^{(t_2)}|jls\rangle &= (-1)^{j+1}5\vec{A}^2 \sum_{\ell} f_{\ell} (2\ell + 1) \sqrt{(2\ell + 1)(2\ell' + 1)} \\
&\cdot \begin{pmatrix} 1 & l & \ell \\ 0 & 0 & 0 \end{pmatrix} \begin{pmatrix} 1 & l' & \ell \\ 0 & 0 & 0 \end{pmatrix} \begin{Bmatrix} 1 & 1 & 2 \\ l & l' & \ell \end{Bmatrix} \begin{Bmatrix} 1 & 1 & 2 \\ l & l' & j \end{Bmatrix}. \tag{H11}
\end{aligned}$$

Substitution for the $\{3j\}$ and $\{6j\}$ symbols gives the results quoted in Eqs.(23-25) in the text.

-
- [1] J.Weinstein and N.Isgur, Phys. Rev. Lett. 48, 659 (1982); Phys. Rev. D27, 588 (1983); Phys. Rev. D41, 2236 (1990).
- [2] K.Dooley, E.S.Swanson and T.Barnes, Phys. Lett. B275, 478 (1992).
- [3] N.Törnqvist, Z. Phys. C61, 525 (1994).
- [4] P.L.Frabetti *et al.* (E687 Collaboration), Phys. Lett. B351, 591 (1995). W.-S.Hou and K.-C.Yang, hep-ph/9911528v3, suggest that FSI effects may also be important in B decays.
- [5] R.Machleidt, K.Holinde and C.Elster, Phys. Rep. 149, 1 (1987). A recent variant of this approach derives NN scattering amplitudes from meson exchange at the quark level; see D.Bartz and Fl.Stancu, hep-ph/0006012.
- [6] There is an extensive literature on the derivation of the NN interaction from quark-gluon forces in the quark model, beginning with D.A.Lieberman, Phys. Rev. D16, 1542 (1977). Most studies have employed resonating group methods (see for example C.S.Warke and R.Shanker, Phys. Rev. C21, 2643 (1980); M.Oka and K.Yazaki, Phys. Lett. 90B, 41 (1980); J.E.T.Ribeiro, Z.Phys.C5, 27 (1980)) and variational methods (for example K.Maltman and N.Isgur, Phys. Rev. D29, 952 (1984)). The Born-order quark-gluon approach described here was applied to NN by T.Barnes, S.Capstick, M.D.Kovarik and E.S.Swanson, Phys. Rev. C48, 539 (1993), and in a closely related approach by D.Hadjimichef, G.Krein, S.Szipigel and J.S.daVeiga, Phys. Lett. B367, 317 (1996).
- [7] M.Lüscher, Comm. Math. Phys. 104, 177 (1986); 105, 153 (1986); Nucl. Phys. B354, 531 (1991); S.R.Sharpe, R.Gupta and G.Kilcup, Nucl. Phys. B383, 309 (1992); R.Gupta, A.Patel and S.R.Sharpe, Phys. Rev. D48, 388 (1993); M.Fukugita *et al.*, Phys. Rev. Lett. 71, 2387 (1993); Phys. Rev. D52, 3003 (1995); S.Aoki *et al.*, hep-lat/9911025. (Fig.5 shows the scattering length quoted by Aoki *et al.*)

- [8] C.Stewart and R.Koniuk, Phys. Rev. D57, 5581 (1998); C.Michael and P.Pennanen, Phys. Rev. D60, 054012 (1999); P.Pennanen, C.Michael and A.M.Green, hep-lat/9908032.
- [9] T.Barnes and E.S.Swanson, Phys. Rev. D46, 131 (1992); see also G.-Q.Zhao, X.G.Jing and J-C.Su, Phys. Rev. D58, 117503-1 (1998); D.Hadjimichef, G.Krein, S.Szpigel and J.S.daVeiga, Phys. Lett. B367, 317 (1996); Ann. Phys. (N.Y.) 268, 105 (1998); B.Masud, J.Paton, A.M.Green and G.Q.Liu, Nucl. Phys. A528, 477 (1991); B.Masud, Phys. Rev. D50, 6783 (1994).
- [10] E.S.Swanson, Ann. Phys. (N.Y.) 220, 73 (1992).
- [11] T.Barnes, E.S.Swanson and J.Weinstein, Phys. Rev. D46, 4868 (1992).
- [12] T.Barnes and E.S.Swanson, Phys. Rev. C49, 1166 (1994); see also D.Hadjimichef, hep-ph/0006330 and nucl-th/9912022.
- [13] T.Barnes, N.Black, D.J.Dean and E.S.Swanson, Phys. Rev. C60, 045202 (1999). The Phys. Rev. C version has an incorrect figure (a duplicate of Fig.4 was used as Fig.5), and minus signs were deleted from the lower y -axis in both figures. The original, archived version nucl-th/9902068 has the correct figures.
- [14] D.Blaschke and G.Röpke, Phys. Lett. B299, 332 (1993); K.Martins, D.Blaschke and E.Quack, Phys. Rev. C51, 2723 (1995); K.Martins, Prog. Part. Nucl. Phys. 36, 409 (1996); D.Blaschke, G.Bureau and Yu.L.Kalinovsky, nucl-th/0006071.
- [15] C.-Y.Wong, E.S.Swanson and T.Barnes, hep-ph/9912431 (Phys. Rev. C to appear); nucl-th/0002034; nucl-th/0006012.
- [16] G.Janssen, K.Holinde and J.Speth, Phys. Rev. C49, 2763 (1994).
- [17] R.Böckmann, C.Hanhart, O.Krehl, S.Krewald and J.Speth, Phys. Rev. C60, 055212 (1999).
- [18] E.Colton *et al.*, Phys. Rev. D3, 2028 (1971).
- [19] N.B.Durusoy *et al.*, Phys. Lett. 45B, 517 (1973).

- [20] W.Hoogland *et al.*, Nucl. Phys. B126, 109 (1977).
- [21] M.J.Losty *et al.*, Nucl. Phys. B69, 185 (1974).
- [22] J.P.Prukop *et al.*, Phys. Rev. D10, 2055 (1974).
- [23] D.Löhse *et al.*, Nucl. Phys. A516, 513 (1990); G.Janssen *et al.*, Phys. Rev. D52, 2690 (1995).
- [24] F.Sassen, personal communication.
- [25] B.Ananthanarayan, G.Colangelo, J.Gasser and H.Leutwyler, hep-ph/0005297.
- [26] S.Weinberg, Phys. Rev. Lett. 17, 616 (1966).
- [27] D.Morgan and M.R.Pennington, “Low Energy $\pi\pi$ Scattering.”, University of Durham report DTP-95/28 (March 1995).
- [28] M.R.Pennington, Nucl. Phys. A623, 189c (1997).
- [29] J.F.Donoghue, C.Ramirez and G.Valencia, Phys. Rev. D38, 2195 (1988).
- [30] N.F.Mott and H.S.W.Massey, *The Theory of Atomic Collisions* (Clarendon Press, Oxford 1965), Sec.VII.8.1.
- [31] T.Barnes and G.I.Ghandour, Phys. Lett. B118, 411 (1982).
- [32] S.Krewald, personal communication.
- [33] Fl.Stancu, D.M.Brink and H.Flocard, Phys. Lett. 68B, 108 (1977).
- [34] D.Mukhopadhyay and H.-J.Pirner, Nucl. Phys. A442, 605 (1985).
- [35] For $\pi_1(1600)$ see V.Dorofeev (VES Collaboration), in Proceedings of WHS99, hep-ex/9905002; G.S.Adams *et al.* (E852 Collaboration), Phys. Rev. Lett. 81, 5760 (1998). For $\pi_1(1400)$ see D.R.Thompson *et al.* (E852 Collaboration), Phys. Rev. Lett. 79, 1630 (1997); A.Abele *et al.* (Crystal Barrel Collaboration), Phys. Lett. B423, 175 (1998); S.U.Chung *et al.* (E852 Collaboration), Phys. Rev. D60, 092001 (1999).

- [36] N.Isgur, R.Kokoski and J.Paton, Phys. Rev. Lett. 54, 869 (1985); T.Barnes, F.E.Close and E.S.Swanson, Phys. Rev. D52, 5242 (1995); C.Bernard *et al.* (MILC Collaboration), Phys. Rev. D56, 7039 (1997); P.Lacock *et al.* (UKQCD Collaboration), Phys. Lett. B401, 308 (1997).
- [37] A.Donnachie and P.R.Page, hep-ph/9807433; Phys. Rev. D58, 114012 (1998).
- [38] M.L.Goldberger and K.M.Watson, *Collision Theory* (J.Wiley, New York 1964).
- [39] Particle Data Group, Review of Particle Properties, Eur. Phys. J. C3, 1 (1998).
- [40] The possibility of measuring this phase using Crystal Barrel $b_1 \rightarrow \omega\pi$ data is being investigated by E.Klempt and B.Pick.
- [41] L.I.Schiff, *Quantum Mechanics* (McGraw-Hill, New York, 1968), pp.384-387.

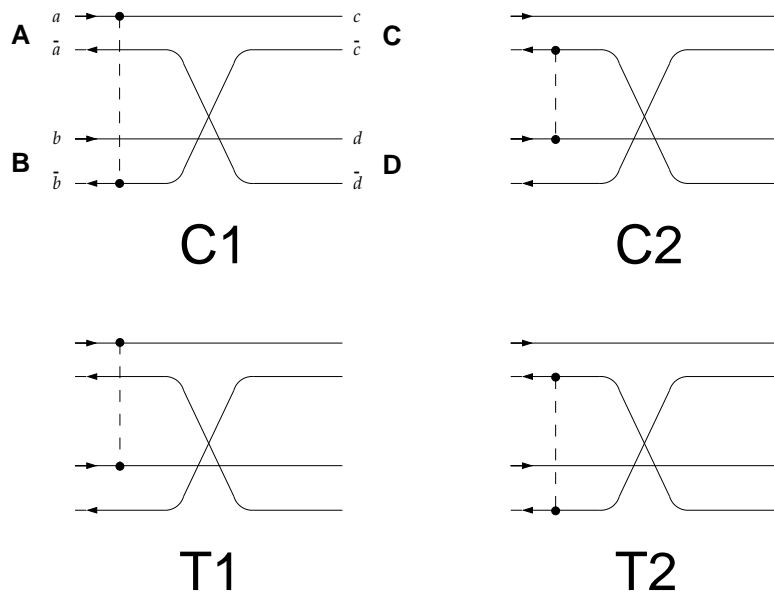


Fig.1. The four quark interchange meson-meson scattering diagrams.

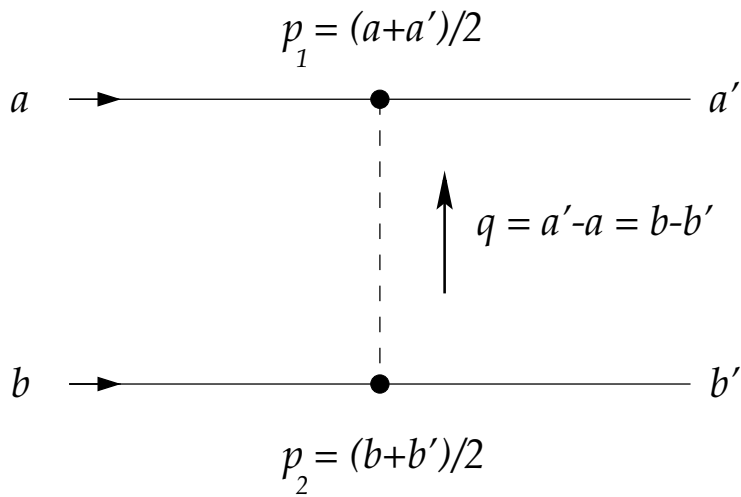


Fig.2. The quark-quark T-matrix, showing three-momentum definitions.

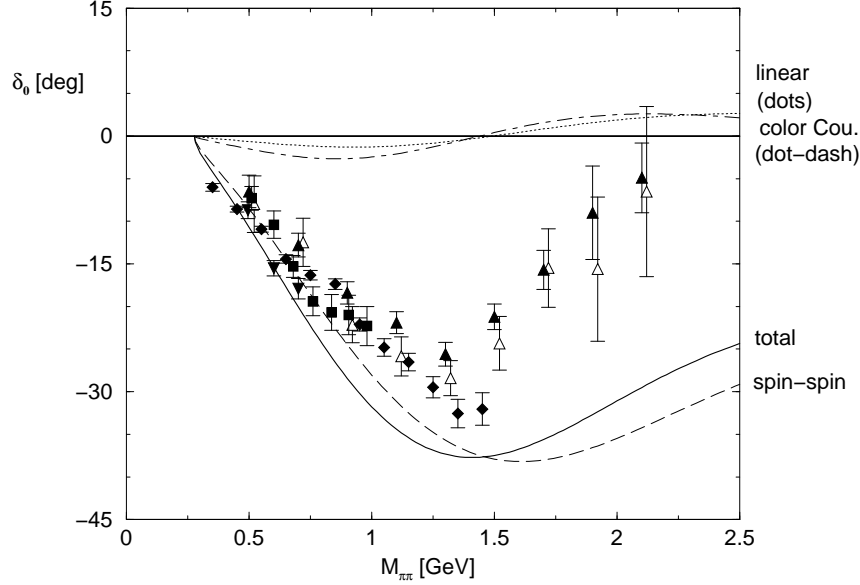


Fig.3. Theoretical contributions to the $I=2$ $\pi\pi$ S-wave phase shift, Eq.(6), with SHO wavefunctions. The experimental phase shifts of Colton *et al.* [18] (down triangles), Durusoy *et al.* [19] (up triangles, two extrapolations), Hoogland *et al.* [20] (set B, diamonds), and Losty *et al.* [21] (squares) are shown.

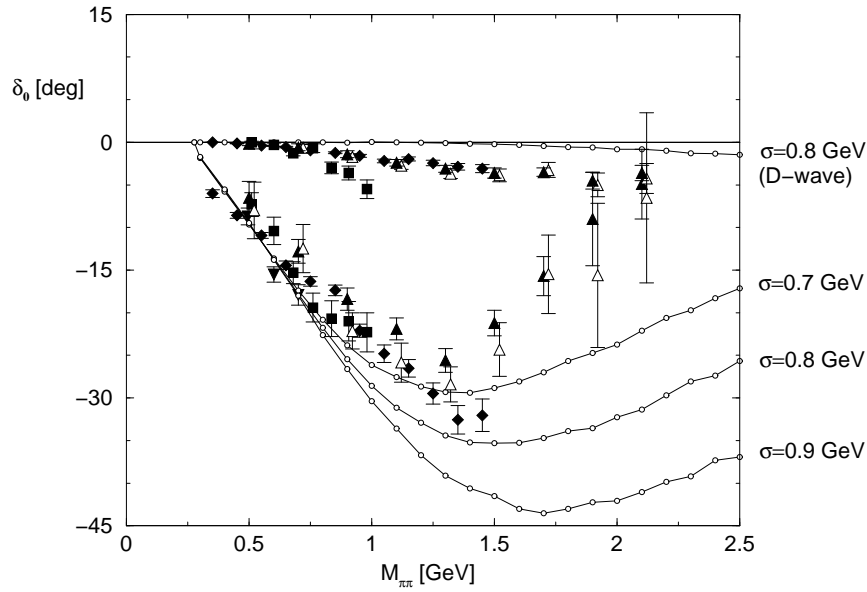


Fig.4. Numerically evaluated $I=2$ $\pi\pi$ S- and D-wave phase shifts with Coulomb plus linear plus hyperfine wavefunctions (lines), compared to experimental phase shifts (symbols as in Fig.3).

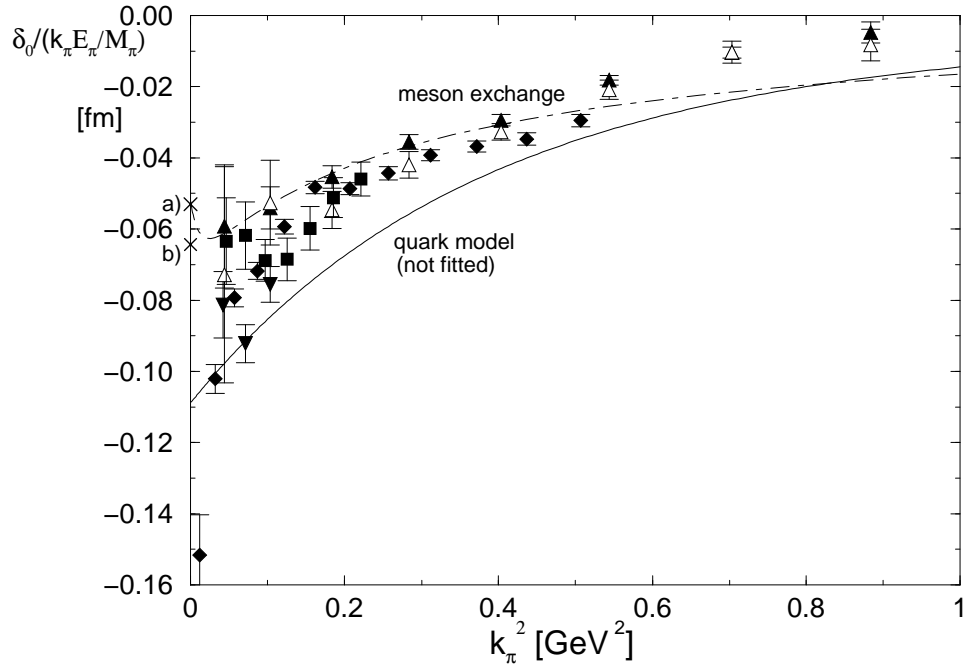


Fig.5. A “generalized specific heat plot” of the $I=2$ $\pi\pi$ S-wave phase shift. The data of Fig.3 is shown together with $a_0^{I=2}$ predictions: a) LGT [7], Roy Eqs. [25], b) PCAC [26], χ PT [29]. Meson exchange [23,24] and quark model (Eq.(6)) predictions are also shown.

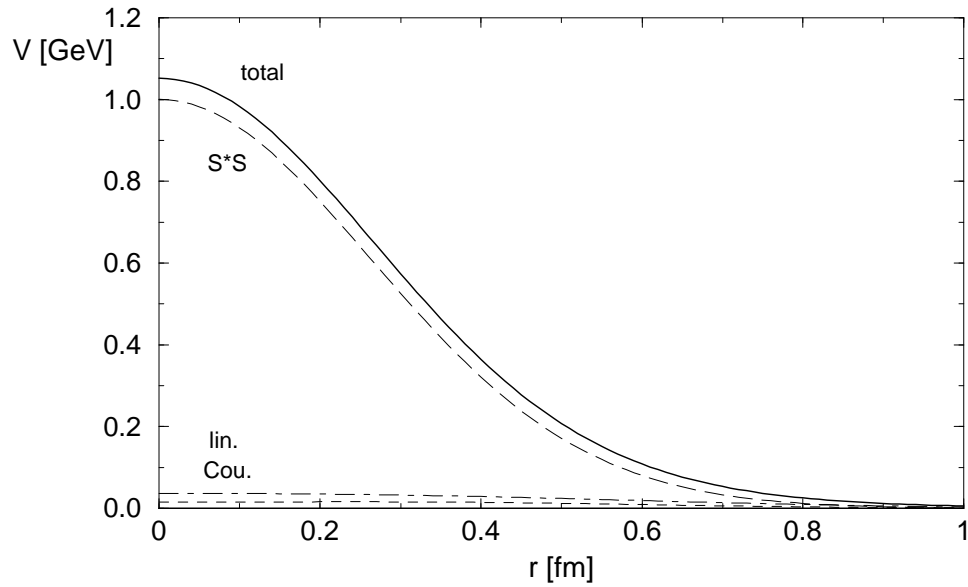


Fig.6. The low energy $I=2$ $\pi\pi$ S-wave potential, Eq.(13).

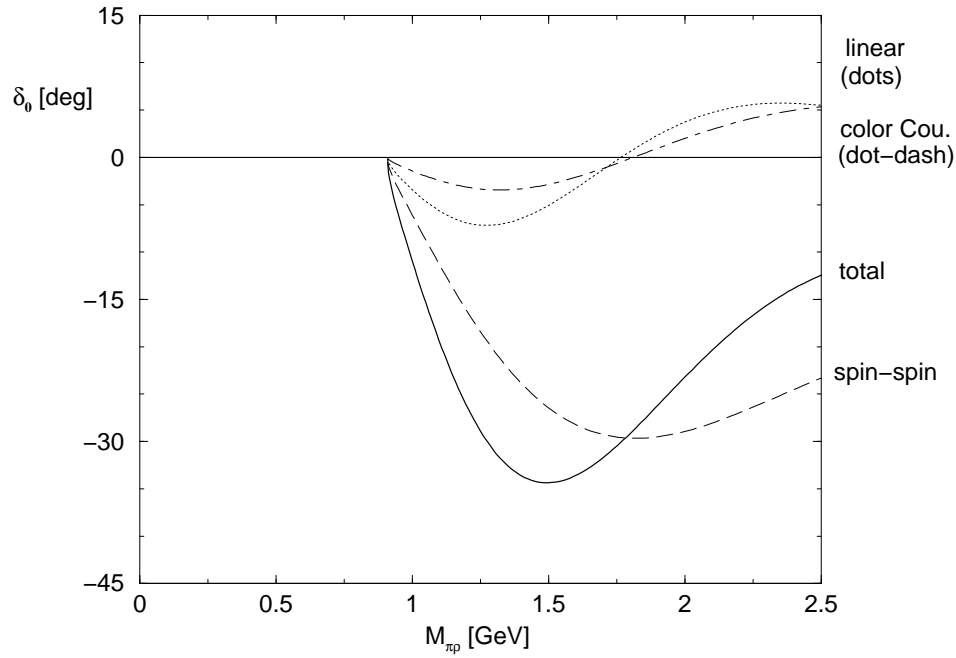


Fig.7. The theoretical $I=2$ $\pi\rho$ S-wave phase shift with SHO wavefunctions, Eq.(28).

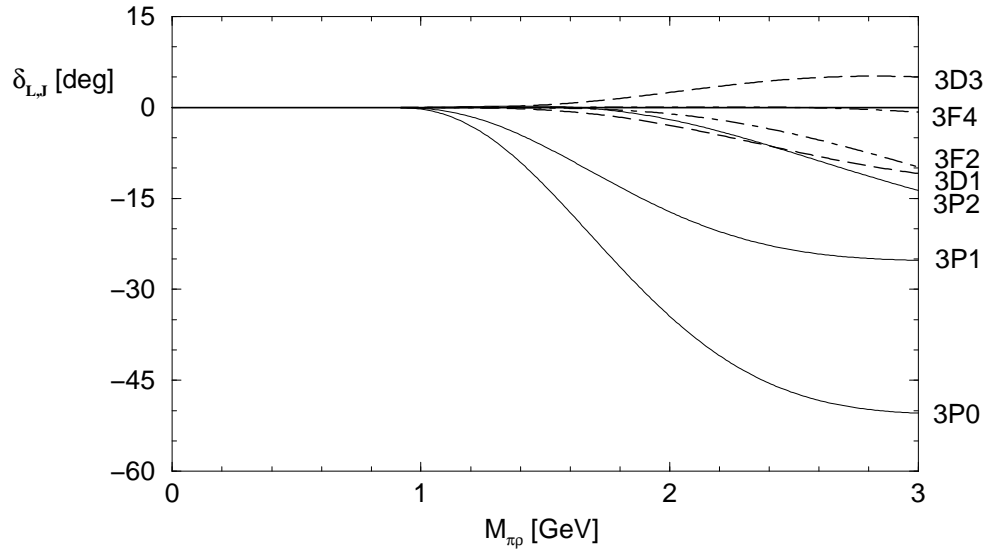


Fig.8. Theoretical $I=2$ $\pi\rho$ phase shifts in P-, D- and F- waves.

3P_2 , 3P_1 , 3P_0 and $J=L\pm 1$ phase shifts are shown.

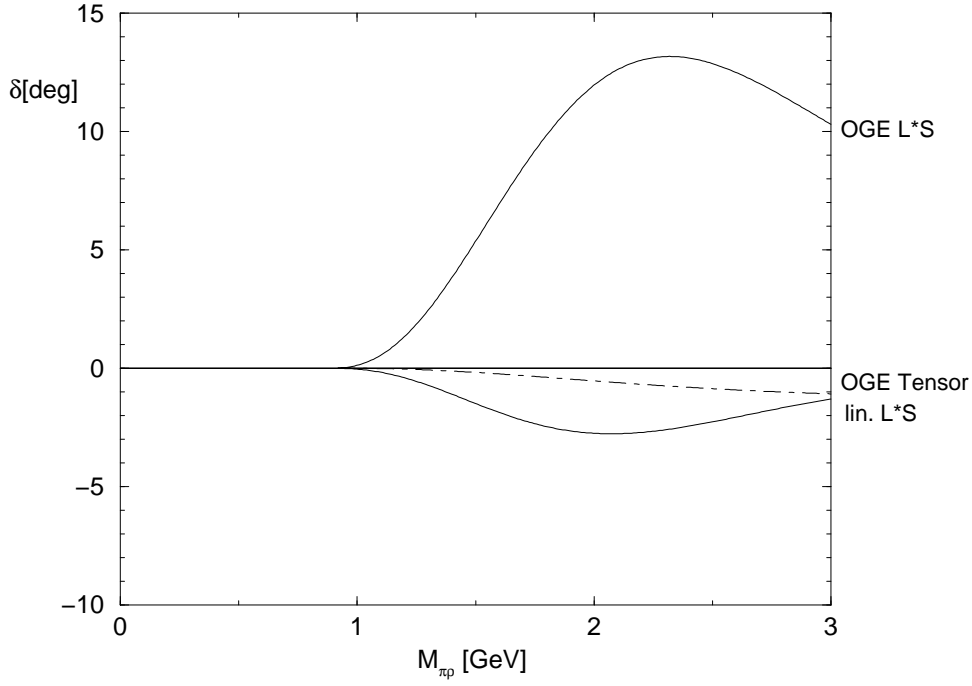


Fig.9. OGE spin-orbit, confining spin-orbit and OGE tensor contributions to the 3P_2 $I=2$ $\pi\rho$ phase shift.

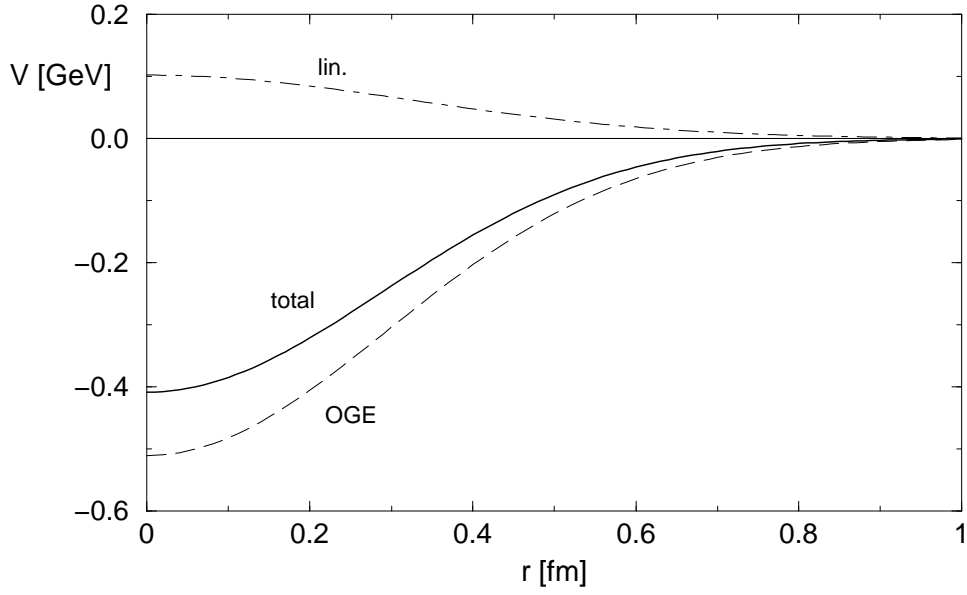


Fig.10. Spin-orbit potentials in the $I=2$ $\pi\rho$ 3P_2 channel, Eq.(29).